U-Pb detrital zircon ages used to infer provenance and tectonic setting of Late Triassic- Miocene sandstones related to the Tethyan development of Cyprus

U-Pb detrital zircon ages used to infer provenance and tectonic setting of Late Triassic-Miocene sandstones related to the Tethyan development of Cyprus

Guohui Chen[1]*, Alastair H. F. Robertson[1] & Timur Ustaömer[2]

[1] School of GeoSciences, University of Edinburgh, West Mains Road, Edinburgh, EH9 3JW, UK

[2] Department of Geology, Istanbul University-Cerrahpaşa, 34320-Avcılar, Istanbul, Turkey

*Correspondence (Guohui.Chen@live.cn)

Abstract

Zircons from Late Triassic deep-water sandstone turbidites of the Mamonia Complex (W Cyprus) have prominent Ediacaran-Cryogenian and Tonian-Stenian-aged populations, with smaller populations at *c.* 2.0 Ga and 2.7-2.5 Ga but only minor concordant Paleozoic zircons. Late Jurassic-Early Cretaceous deep-water gravity-deposited sandstone, also from the Mamonia Complex, has a greater proportion of Ediacaran-Cryogenian and Tonian-Stenian zircons, but less abundant Paleoproterozoic, Archean and Paleozoic ones. Similar zircon populations characterise an Early Cretaceous shallow-marine sandstone block in the Moni Melange (S Cyprus). The dominant Ediacaran-Cryogenian and Tonian-Stenian zircon populations originated in the NE Africa/Arabian-Nubian Shield (N Gondwana). However, they were probably recycled from Paleozoic sandstones within Anatolia following South Neotethyan rifting that also gave rise to sparse Permian-Triassic zircons. Paleozoic zircons reflect Variscan magmatism within Anatolia. Both Late Cretaceous and overlying Eocene sandstone turbidites in the Kyrenia Range (N Cyprus) contain prominent Ediacaran-Cryogenian populations, together with small Archean, Tonian, Carboniferous and Late Cretaceous populations, with additional Triassic zircons in the Eocene sample. Late Cretaceous zircons dominate an overlying Late Miocene sandstone turbidite, together with minor Ediacaran-Cryogenian, Eocene and Miocene populations. The Late Cretaceous zircons record continental margin arc and/or ophiolite-related magmatism, whereas Eocene and Miocene zircons represent collision-related magmatism, both in S Turkey.

Supplementary materials: Detailed zircon U–Pb geochronological data and supplementary figure are available at XXXX.

Detrital zircon dating aids understanding of the tectonic development of Tethys in the Eastern Mediterranean area, as elsewhere (Zulauf *et al.* 2007; Ustaömer *et al.* 2014; Avigad *et al.* 2015; Buckman *et al.* 2018). Cyprus is best known for the Late Cretaceous (*c.* 90 Ma) Troodos ophiolite (Gass 1968, 1990; Moores & Vine 1971; Pearce 1975; Mukasa & Ludden 1987; Robinson & Malpas 1990; Robertson 2002) that formed within the Southern Neotethys. An understanding of the tectonic setting of the ophiolite depends on taking account of the sedimentary provenance of two adjacent allochthonous terranes. The first is the Mamonia Complex in west Cyprus, together with the related Moni Melange in south Cyprus (Lapierre 1975; Robertson 1977; Robertson & Woodcock 1979). The second is the Kyrenia Range in northern Cyprus (Ducloz 1972; Baroz 1979; Robertson & Woodcock 1986) (Fig. 1). The two allochthonous crustal units also need to be considered in the wider context of North Africa to the south and the mosaic of continental, ophiolite-related and magmatic arc-related units that make up Anatolia, including the Taurides in the south and the Pontides in the north (Okay & Tüysüz 1999) (Fig. 2).

The depositional ages of the sedimentary successions associated with the Mamonia Complex and the Kyrenia Range are mainly well known, based on micropaleontological studies and some strontium isotope dating (e.g. Baroz 1979; Urquhart & Banner 1994; Hakyemez *et al.* 2000; Lord *et al.* 2000; McCay *et al.* 2013). The facies and petrography of these units have been extensively studied and combined with other geological and geophysical evidence to produce regional tectonic reconstructions (McCay & Robertson 2012; Robertson *et al.* 2012*a*; Torley & Robertson 2018). However, conventional petrographic studies do not indicate the age of source constituents. In this paper, we provide the first high-quality radiometric age data of detrital zircons from Late Triassic and Cretaceous sandstones from the Mamonia Complex (and the Moni Melange), and also from Late Cretaceous-Miocene sandstones from the Kyrenia Range. Our results emphasize the contribution of detrital zircon dating to regional provenance analysis and tectonic reconstruction, while also highlighting the complexities inherent in any region involving the dispersal and amalgamation of continental fragments, such as characterise the Tethyan orogen.

Role of detrital zircon dating

There are four main ways in which detrital zircon dating can shed light on Tethyan development in the Cyprus region: (1) to help constrain the maximum age of sediment deposition; i.e., the youngest detrital zircon ages will be compared to existing age data; (2) to identify sedimentary provenance by comparing the ages of tectono-thermal events recorded in the zircon grains with possible source units; e.g. major cratons, epi-cratonic basins and peri-Gondwanan terranes; (3) to help identify sedimentary provenance by comparison of zircon ages with known igneous events in the region,

notably ophiolite genesis, subduction-related arc magmatism and collision-related volcanism in the surrounding region; and (4) to test, and if appropriate, modify existing tectonic models of the Mesozoic-Cenozoic Tethys in the easternmost Mediterranean region.

Regional geological setting

Cyprus is a microcosm of Tethys because it includes remnants of: (1) a rifted passive margin in the form of the Triassic-Cretaceous Mamonia Complex in west Cyprus and the related Moni Melange in south Cyprus; (2) supra-subduction zone (SSZ)-oceanic crust represented by the Late Cretaceous Troodos ophiolite; and (3) An active (convergent) margin represented by the latest Cretaceous-Neogene rocks of the Kyrenia Range, north Cyprus (Fig. 1). The easternmost Mediterranean region and Anatolia include the remnants of several Mesozoic oceanic basins, including the Southern Neotethys (Şengör 1984; Robertson & Dixon 1984; Stampfli & Borel 2002; Göncüoğlu *et al.* 2003; Barrier *et al.* 2018). The Southern Neotethys is widely considered to have formed by rifting of the northern margin of Gondwana during Late Permian-early Mesozoic time (Şengör 1984; Robertson & Dixon 1984; Stampfli & Borel 2002; Göncüoğlu *et al.* 2003). The Southern Neotethys closed during Late Cretaceous-early Cenozoic time probably related to northward subduction (Şengör & Yılmaz 1981; Robertson & Dixon 1984; Barrier *et al.* 2018). Remnants of the Southern Neotethys including ophiolites in SE Turkey were emplaced onto the northern margin of the North African-Arabian Plate as a consequence of Late Cretaceous subduction and subsequent trench-passive margin collision. However, the Troodos ophiolite remained in a remnant oceanic basin during the Cenozoic. The ophiolite was emplaced against Tauride continental crust to the north by the Late Miocene-Early Pliocene (Harrison *et al.* 2004; McCay & Robertson, 2013; Robertson *et al.* 2014) and collided with the leading edge of African continental crust represented by the Eratosthenes Seamount during the Plio-Quaternary with corresponding uplift of the Troodos Massif (Robertson, 1998).

Mamonia Complex/Moni Melange

The entirely sedimentary Ayios Photios Group of the Mamonia Complex in west Cyprus encompasses the Late Triassic Vlambouros Formation, the Late Triassic Marona Formation and the Late Triassic-Early Cretaceous Episkopi Formation (Robertson & Woodcock 1979; Torley & Robertson 2108) (Figs. 3, 4). The Vlambouros Formation is characterised by grey, thin, medium and thick-bedded turbiditic sandstones, intercalated with siltstones/mudstones, together up to 30 m thick (Lapierre 1975; Robertson & Woodcock 1979; Torley & Robertson 2018). The Marona Formation, where present, depositionally overlies the Vlambouros Formation (e.g. Dhiarizos Valley), where it comprises bioturbated hemipelagic limestones and mudstones, up to 25 m thick (Lapierre 1975;

Robertson & Woodcock 1979; Torley & Robertson 2018). The overlying deep-water Episkopi Formation (as redefined by Torley & Robertson, 2018) comprises non-calcareous reddish mudstones, shales, metalliferous sediments, ribbon-bedded radiolarites and redeposited shallow-water carbonates, together with fine to medium-bedded quartzose sandstones (Robertson & Woodcock 1979; Torley & Robertson 2018). The upper part of the succession is characterised by locally distributed, medium to coarse-grained quartzose sandstones (Akamas Member), that are locally very thick-bedded (e.g. Akamas Peninsula) (Robertson & Woodcock 1979).

In addition, the related Moni Melange of southern Cyprus (Fig. 5) includes two allochthonous components. First, there are detached blocks of Mamonia Complex-type rocks including alkali basalt, radiolarite and pelagic limestone. Large detached blocks of Early Cretaceous-aged shallow-marine quartzose sandstone (*c.* 60 m thick) are known as the Pareklisia Member. Secondly, there are thrust sheets of serpentinite associated with emplacement of the Troodos oceanic lithosphere (Robertson 1977).

During this study, detrital zircons were dated from sandstones of the Late Triassic Vlamborous Formation, the Late Jurassic-Early Cretaceous Akamas Member (Episkopi Formation) and the Early Cretaceous Pareklisia Member.

Kyrenia Range

The intact stratigraphy the Kyrenia Range (Fig. 6) begins with the Trypa (Tripa) Group, *c.* 700 m thick, which is dominated by Triassic-Cretaceous shallow-marine carbonates. These lithologies were brecciated, recrystallized and regionally metamorphosed to greenschist grade during the Late Cretaceous (Ducloz 1972; Baroz 1979; Robertson & Woodcock 1986). The Trypa (Tripa) Group is unconformably overlain by the Campanian-Middle Eocene Lapithos (Lapta) Group (up to *c.* 1500 m thick), which is mainly carbonate breccias, pelagic carbonates, basic volcanics and calcareous sandstones. Unconformably above comes a very thick (up to *c.* 4000 m), variably deformed succession of dominantly siliciclastic sedimentary rocks, mainly conglomerates, sandstone turbidites and mudstones, forming the Late Eocene-Late Miocene Kythrea (Değirmenlik) Group (Fig. 6) (Baroz 1979; Hakyemez *et al.* 2000; McCay & Robertson 2012; McCay *et al.* 2013). The intact succession ends with Messinian evaporites and was followed by southward-directed thrusting during latest Cretaceous-earliest Pliocene time, related to regional continental collision (McCay & Robertson 2013; Robertson & Kinnaird, 2016).

During this work, detrital zircons were analysed from sandstone turbidites of the Late Campanian-Maastrichtian Kiparisso Vouno (Alevkaya Tepe) Member and the Middle Eocene Kalograia-Ardana (Bah çeli–Ardahan) Formation (Lapithos (Lapta) Group), the Late Miocene Davlos

(Kaplıca) Formation and the Middle-Late Miocene Mia Milia (Dağyolu) Formation (Kythrea (Değirmenlik) Group).

Analytical methods

Zircon separation

The zircon separation followed previously reported procedures (McLennan *et al.* 2001; Fedo *et al.* 2003; Ustaömer P. A. *et al.* 2012*a*), with slight modifications. Approximately 10 kg of sandstone were collected from each typical medium to coarse-grained sandstone. A polished thin-section was made from each sample for optical microscope examination. The samples were crushed and sieved using 4 meshes of 63 to 500 μm to maximize detrital zircon recovery. The heavy minerals were concentrated hydrodynamically using a Wilfley table, then washed and dried. A hand magnet was used to remove strongly magnetic minerals. Less magnetic minerals were then removed using a Frantz Isodynamic magnetic separator at progressively higher magnetic currents (0.4, 0.8 and 1.5 amps), with side slopes of 20° and tilt of 25°. Non-magnetic heavy minerals were next gravitationally separated using the heavy liquid, lithium polytungstate (specific gravity: 2.85 g/ml). For each sample, ~150-200 zircon grains were randomly picked under a binocular microscope, mounted in epoxy resin and polished sufficiently to expose the centre of the grains.

Scanning electron microscopy

Zircon morphology and internal micro-texture were observed, using cathodoluminescence (CL), with a Carl Zeiss SIGMA HD VP Field Emission Scanning Electron Microscope (SEM) at the School of GeoSciences, University of Edinburgh. Back-scattered electron detector (BSED) images were used to examine zircon morphology (including inclusions).

SIMS U-Pb dating of zircon

U-Pb isotopic measurements were made on a CAMECA ims-1270 SIMS at the Edinburgh Ion Microprobe Facility (EIMF), in the Material and Micro-Analysis Centre (EMMAC) of the School of GeoSciences, University of Edinburgh using the methods detailed by Kelly *et al.* (2008) and Ustaömer P. A. *et al.* (2012*b*). U/Pb ratios were calibrated against measurements of the Geostandard 91500 zircon (~1062.5 Ma) (Wiedenbeck *et al.* 1995). Measurements over a single 'session' (a period during which no tuning or changes to the instrument took place) gave a standard deviation of *c.* 1σ (1%) for $^{206}Pb/^{238}U$ measurements, for individual repeats of 91500. Rapid ('short protocol') analysis (7 minutes per analysis) was used, in which pre-sputter was limited to 60 seconds and measurements to peaks of Zr_2O (all four lead isotopes), ThO_2 and UO_2. Eight cycles were measured

(none were excluded). The 91500 standard was re-analysed after every 10 measurements. Correction for in situ common Pb was made using measured ^{204}Pb counts above that of the detector background and modern-day common Pb composition. The modern Pb correction assumes that in nearly all cases measured common Pb results from contamination on the sample surface and in exposed cracks.

Age determinations were derived from the U-Th-Pb isotope data (632 analyses), of which 578 were 90-110% concordant. Six of the eight samples analysed (80-100 randomly analysed zircons) provide significant detrital zircon age distributions (e.g. Andersen 2005). The remaining two samples have fewer analyses because few zircons could be separated; these are viewed as exploratory data. Full isotopic results are given in supplementary material Table S1.

Data reduction utilised geochronological plots that were produced using ISOPLOT spreadsheets (Ludwig 2012) and AgeDisplay (Sircombe 2004). The International Chronostratigraphic Chart of the International Commission on Stratigraphy (Cohen *et al.* 2018) is used here for the timescale.

Sampling and petrography

Mamonia Complex & Moni Melange

Vlambouros Formation

Two samples of medium to coarse-grained sandstone were analysed from the Late Triassic Vlambouros Formation (W Cyprus). Sample GC14-3 (GPS: 34°46′55″ N, 32°31′33″ E) is a thin to medium-bedded sandstone turbidite from the upper part of the Vlambouros Formation, south of Episkopi village (Fig. 4). Sample GC14-9 (GPS: 34°58′33″ N, 32°21′39″ E) is a medium to thick-bedded sandstone turbidite from the upper part of the formation, south of Fasli (Fig. 4). Both sandstones have angular to sub-angular, poorly to moderately sorted grains, with a grain-supported texture, set in a micritic matrix. Quartz grains predominate, commonly with undulose extinction, together with plagioclase, orthoclase, hornblende, epidote, muscovite and occasional heavy minerals (including zircon) and opaque grains. Lithic fragments include metamorphic quartzite (Torley & Robertson 2018).

Akamas Member

Sample GC14-16 (GPS: 34°51′37″ N, 32°36′18″ E) is a thick-bedded, coarse-grained quartzose sandstone (grains up to 3 mm in diameter) of Late Jurassic-Early Cretaceous age, from near Ayios Photios (Fig. 4). This sandstone has sub-rounded to well-rounded grains that are moderately to well-sorted with a grain-supported texture. Quartz dominates, with occasional very fine-grained quartzite, microcline, plagioclase and muscovite (Torley & Robertson 2018).

194 *Pareklisia Member (Moni Melange)*

195 Sample GC14-17 (GPS: 34°44′09″ N, 33°09′27″ E) was collected from a detached block of medium
196 to coarse-grained, pale-yellow, poorly cemented, cross-bedded, pebbly quartzose sandstone of the
197 Early Cretaceous Pareklisia Member, from south of Pareklisia village (Fig. 5). The sandstone is
198 petrographically similar to the Akamas Member of the Mamonia Complex (Robertson 1977;
199 Swarbrick & Robertson 1980). The grains are sub-angular to sub-rounded and poorly sorted, with a
200 grain-supported texture. Quartz grains predominate, with occasional feldspar, hornblende, muscovite
201 and zircon (Robertson 1977).

202 ***Kyrenia Range***

203 *Kiparisso Vouno (Alevkaya Tepe) Member*

204 A sandstone turbidite, sample GC14-47 (GPS: 35°19′40″ N, 33°08′28″ E), was collected from the
205 Late Campanian-Maastrichtian type section of this member, to the north of the E-W ridge-crest road
206 (Fig. 7). This sample is dominated by monocrystalline and polycrystalline quartz and muscovite
207 schist, together with rare, angular fragments of basalt, angular to sub-rounded grains of red
208 radiolarian chert, red mudstone, pyroxene and biotite. Bioclastic detritus, includes plankic
209 foraminifera and echinoderm debris (Robertson *et al.* 2012*b*).

210 *Kalograia-Ardana (Bahçeli–Ardahan) Formation*

211 Sample GC14-32 (GPS: 35°22′25″ N, 33°51′58″ E) is an Eocene-aged, normal-graded sandstone
212 turbidite from the Mersinlik (Flamoudi) area, eastern Kyrenia Range (Fig. 7). The sandstone has
213 sand-sized, angular to subangular, ophiolite-derived grains, mainly serpentinite, with common red
214 radiolarian chert and minor basalt. Terrigenous grains include unstrained quartz, muscovite, biotite
215 and lithic grains (e.g. siltstone, quartzite, schist and limestone). Bioclastic grains include fragmented
216 benthic foraminifera and bivalve shells; carbonate intraclasts are also present (Robertson *et al.* 2014).

217 *Davlos (Kaplıca) Formation*

218 Sample GC14-25 (GPS: 35°20′40″ N, 33°34′44″ E) is a Late Miocene, medium-grained sandstone
219 turbidite, from west of Bahçeli (Kalograia) (Fig. 7). The sandstone is poorly-sorted, medium-grained
220 and contains angular to sub-rounded grains of quartz (mainly monocrystalline), plagioclase and
221 carbonate rocks, together with igneous rock fragments (e.g. serpentinite, diabase) and metamorphic
222 rock fragments (e.g. muscovite schist). Rare benthic and planktic foraminiferal fragments are also
223 present (McCay & Robertson 2012).

Mia Milia (Dağyolu) Formation

Sample GC14-36 (GPS: 35°18′52″ N, 33°43′50″ E) was collected from a thick-bedded sandstone in the higher levels of the Middle-Late Miocene Mia Milia (Dağyolu) Formation, near Arıdamı (Artemi) (Fig. 7). The sandstone comprises relatively well-sorted grains of quartz, igneous lithic fragments and carbonates. Metamorphic lithic grains (e.g. muscovite schist) occur in small amounts, together with rare opaque grains (McCay & Robertson 2012).

Geochronological results

Mamonia Complex & Moni Melange

Vlambouros Formation

Zircons are abundant, varying in size and opacity. The grains range from rounded to stubby prisms and slightly elongate prisms (e.g. Fig. 8a: grains 25, 54 and 83; Fig. 8b: grains 8-9, 39-41). Individual zircon crystals vary in length from 70-200 μm. Most zircons exhibit oscillatory zoning in CL images (e.g. Fig. 8a: grains 25, 37, 49 and 83; Fig. 8b: grains 40, 43 and 65) but a few lack compositional zoning or show patchy zoning (e.g. Fig. 8a: grains 15 and 53; Fig. 8b: grains 39, 46 and 57). Inherited cores occur rarely (e.g. Fig. 8a: grain 12; Fig. 8b: grain 8).

In sample GC14-3, most zircons have relatively high Th/U ratios (>0.1) (see supplementary material Table S1), suggesting a magmatic derivation (Rubatto 2002; Teipel *et al.* 2004). Lower Th/U ratio (Th/U<0.1) occur in three grains, together with relatively dark CL images showing metamict cores (Fig. 8a: grains 12 and 46) and faint internal structures (Fig. 8a: grain 43). Concordance-filtered (90-110%) zircon ages indicate a polymodal age distribution, with major groups of 548-635 Ma (Ediacaran; 14%), 637-691 Ma (Cryogenian; 14%), 724-999 Ma (Tonian; 36 %), 1037-1188 Ma (Stenian; 6%), 1839-2020 Ma (Orosirian; 9%) and 2512-2745 Ma (Neoarchean; 9%) (Fig. 9a-b). 1.2-1.8 Ga-aged zircons are represented by only two grains (1240 and 1409 Ma, respectively). An age gap of 2.1-2.5 Ga is observed (Fig. 9b; see supplementary material Figure S1), with one exception (grain 72), with an age of 2151 Ma. The youngest concordant zircon grain is subhedral (Fig. 8a: grain 25), with a $^{206}Pb/^{238}U$ age of *c.* 320 Ma (mid-Carboniferous).

Zircons from sample GC14-9 mainly have high Th/U ratios (>0.14) (see supplementary material Table S1), with the exception of grains 47 and 57 (Th/U=0.02-0.03) that have homogeneous dark CL images (Fig. 8b). The population age ranges are 505-537 Ma (Cambrian; 10%), 549-630 Ma (Ediacaran; 15%), 639-705 Ma (Cryogenian; 10%), 759-987 Ma (Tonian; 33%) and 1009-1095 Ma (Stenian; 15%) (Fig. 9c-d). Comparable age gaps of *c.* 1.1-1.8 Ga and 2.1-2.6 Ga are present in this sandstone (Fig. 9d) (see supplementary material Figure S1), other than grains 83 (1.66 Ga), 85 (2.21

Ga) and 3 (2.42 Ga) (see supplementary material Table S1). The youngest relatively concordant age is 525 Ma (Cambrian; Fig. 8b: grain 46).

Akamas Member

Sample (GC14-16) contains abundant zircons that are mostly subhedral to subrounded and variably sized (100-250 μm). CL images (Fig. 8c) exhibit various internal structures, including core-mantle structure (e.g. Fig. 8c: grains 1, 88), banded zonation (Fig. 8c: grain 39) and common oscillatory zoning (Fig. 8c: grains 8, 21). Most grains have Th/U ratios of >0.1 (see supplementary material Table S1), with two exceptions; of these, grain 42 has a dark, irregular inherited core (i.e. metamict), whereas grain 88 has a bright, sub-rounded inherited core with a dark structureless rim (Fig. 8c). Concordance-filtered (90-110%) zircon populations cluster mainly in the Neoproterozoic, with components of 578-633 Ma (Ediacaran; 27%), 636-713 Ma (Cryogenian; 29%), 725-1000 Ma (Tonian; 32%) and 1018-1094 Ma (Stenian; 7%) (Fig. 10a-b). Smaller age groups occur at 2560-2607 Ma (Neoarchean; 2%). The youngest 100% concordant age is 588 Ma (Ediacaran). Only one grain (no. 17; 2034 Ma) is in the *c.* 1.1-2.5 Ga range (Fig. 10b).

Pareklisia Member (Moni Melange)

The zircons are 80-250 μm long, subhedral (e.g. Fig. 8d: grains 3, 40) to rounded (e.g. Fig. 8d: grain 59). Most grains exhibit igneous-derived oscillatory zonation (e.g. Fig. 8d: grains 3, 87) (Corfu *et al.* 2003). Core-mantle structures are common, with various internal patterns and colours (e.g. Fig. 8d: grains 27, 82). Inherited protolith cores are generally surrounded by concentric pale to dark-grey rims (e.g. Fig. 8d: grain 86). Common rounding is inferred to have resulted from abrasion during long-distance sedimentary transport or sedimentary recycling (e.g. Corfu *et al.* 2003; Ustaömer *et al.* 2013). The zircons (90-110% concordant) group at 571-633 Ma (Ediacaran; 25%), 638-719 Ma (Cryogenian; 27%), 766-981 Ma (Tonian; 25%) and 1004-1126 Ma (Stenian; 13%) (Fig. 10c-d). The youngest 100% concordant age is 630 Ma (Ediacaran). There is a wide age gap from *c.* 1.1 Ga to 2.6 Ga (Fig. 10d; see supplementary material Figure S1), other than a 2.0 Ga for one grain (no. 88; see supplementary material Table S1).

Comparison of zircon populations

The Mamonia Complex and Moni Melange sandstones are dominated by Late Neoproterozoic zircon populations. Ediacaran-Cryogenian and Tonian-Stenian zircon populations dominate the sandstones of the Vlambouros Formation, specifically. The sandstone of the Akamas Member has similar but more age-restricted zircon populations (Figs. 9-10; see supplementary material Figure S1). The sandstones of the Pareklisia and Akamas Member share similar Late Neoproterozoic and Tonian-

Stenian zircon populations. Zircon populations of *c.* 1.1-1.8 Ga and *c.* 2.0-2.5 Ga are absent in both units, although a few grains lie within these age ranges (Fig. 9-10; see supplementary material Figure S1). Minor Paleozoic zircon populations in sandstones of the Vlambouros Formation mainly cluster in the Cambrian, together with sparse zircons of Ordovician, Devonian, Carboniferous and Permian ages. Of these, 13 out of 32 grains have reliable (90-110%) concordance levels.

Kyrenia Range

Kiparisso Vouno (Alevkaya Tepe) Member

Zircon grains range from mainly subhedral to subrounded to rounded, and range from 50 to 230 μm long. CL images reveal detrital cores, generally enclosed by concentric oscillatory zonation (Fig. 8e: grains 2 and 4). The zircons typically have relatively high Th/U ratios (>0.1; see supplementary material Table S1), consistent with an igneous origin (Rubatto 2002; Teipel *et al.* 2004). A single zircon has a Th/U ratio of 0.01 (no. 103; see supplementary material Table S1), suggestive of a metamorphic origin (e.g. Rubatto 2002). Concordant ages dominantly group at 551-615 Ma (Ediacaran; 13%), 646-702 Ma (Cryogenian; 8%), 729-1091 Ma (Tonian-Stenian; 25%), 1849-2045 Ma (Orosirian; 13%) and 2542-2701 Ma (Neoarchean; 9%) (Fig. 11a-b). Paleozoic zircons (<541 Ma; 36 grains) mainly cluster in the Carboniferous (312-346 Ma), Late Silurian (*c.* 422 Ma) and Ordovician (451-475 Ma); of these, six grains provide highly reliable 97-103% concordant ages (Fig. 11a-b; see Discussion). There is also a minor *c.* 98% concordant Late Cretaceous (87 and 95 Ma) fraction (Fig. 8e: grain 4). The youngest 100% concordant zircon is Ordovician (461 Ma). There is a large age gap from 1.1 to 1.8 Ga, and a small age gap between *c.* 2.1-2.5 Ga (with only 3 concordant ages) (Fig. 11b; see supplementary material Figure S1).

Kalograia-Ardana (Bahçeli–Ardahan) Formation

Zircon crystals are mainly rounded to subrounded to subhedral, from 40-300 μm long. Core-mantle structure and oscillatory zoning are seen in most CL images (e.g. Fig. 8f: grains 3, 12, 56 and 80). Inherited cores are generally surrounded by a pale-grey rim with concentric zoning or weak zoning (e.g. Fig. 8f: grains 3, 74). The zircons typically have relatively high Th/U ratios, ranging from 0.14-2.74 (see supplementary material Table S1), suggesting a magmatic origin (Rubatto 2002). A single rounded grain with a low Th/U ratio (Th/U=0.04) has an irregular dark, inherited core and a pale-grey, unzoned outer rim (Fig. 8f: grain 74), indicative of a metamorphic event (e.g. Rubatto 2002; Corfu *et al.* 2003). Concordant (90-100%) ages of significant zircon populations range from 559-620 Ma (Ediacaran; 15%), 647-705 Ma (Cryogenian; 10%), 753-999 Ma (Tonian; 22%) and 1040-1140 Ma (Stenian; 7%), with age gaps from *c.* 1.1-2.1 Ga and 2.2-2.7 Ga (Fig. 11c-d; see supplementary

material Figure S1). There are also trace, to minor, zircon fractions with Paleozoic (311-363 Ma; Late Devonian-Late Carboniferous), Mesozoic (219-232 Ma; Triassic and 87-94 Ma; Late Cretaceous) and Cenozoic (61 Ma; Paleocene and 45 Ma; Eocene) ages (Fig. 11c). The youngest 100% concordant age is 45 Ma (Eocene) (Fig. 8f: grain 56).

Davlos (Kaplıca) Formation

Detrital zircons are mostly colourless or brownish, euhedral to rarely subhedral or rounded (e.g. Fig. 8g: grain 13), ranging from 130-250 μm in length. CL images reveal common oscillatory zoning (e.g. Fig. 8g: grains 1, 7 and 11) suggesting a magmatic origin (Corfu *et al.* 2003); other zircons have inherited, irregular cores and concentrically zoned or structureless rims (e.g. Fig. 8g: grains 22, and 30). Th/U ratios are typically >0.15 (see supplementary material Table S1), consistent with an igneous origin (e.g. Rubatto 2002). Concordant zircons are characterised by ages of 71-91 Ma (Late Cretaceous; peaks of 74 and 84 Ma; 83% of total), with minor fractions of 689-1017 Ma (Neoproterozoic; 10%), *c.* 51 Ma (Eocene; 2%) and *c.* 21 Ma (Miocene; 2%) (Fig. 12a-b; see supplementary material Figure S1). The youngest 100% concordant zircon age is 74 Ma (Late Cretaceous; Fig. 8g: grain 30).

Mia Milia (Dağyolu) Formation

Most zircons are euhedral (Fig. 8h) and 120-280 μm in length. Core-mantle structure is common; where present, inherited cores are rimmed by fine oscillatory zonation (e.g. Fig. 8h: grains 5, 6), or dark structureless zircon (e.g. Fig. 8h: grain 3). Th/U ratios are >0.1 (see supplementary material Table S1), suggesting an igneous origin (e.g. Rubatto 2002). Only six dateable zircon grains could be extracted, yielding ages of 13-16 Ma (Miocene), 24-25 Ma (Oligocene) and 558-813 Ma (Ediacaran-Tonian) (Fig. 12c-d). None of these zircons have 100% concordance. The youngest age is 13 Ma (Serravallian) (grain 3; Fig. 8h).

Comparison of zircon populations

The Kyrenia Range sandstones are characterised by Ediacaran-Cryogenian and Paleoproterozoic zircons, with a minor fraction of Tonian-Stenian ages. Paleozoic, Mesozoic and Cenozoic zircon populations generally increase in sandstones of younger depositional age (Figs. 11-12; see supplementary material Figure S1). Late Cretaceous (Turonian-Campanian) zircons form a significant age population in the Cenozoic sandstones. Cenozoic zircons are rarely present in the Eocene and Late Miocene sandstones. Age gaps of *c.* 1.1-2.1 Ga and 2.2-2.7 Ga exist in the Late Cretaceous and Eocene samples (see supplementary material Figure S1), in contrast to the Late Miocene one, although few grains were analysed in these sandstones.

Discussion

Depositional age based on zircon geochronology

After formation and cooling by igneous or metamorphic processes, detrital zircons were eroded, transported and deposited to form the sandstones studied. For extrusive igneous rocks this requires only erosion and deposition. However, for intrusive igneous rocks and metamorphic rocks, variable exhumation is required prior to erosion and deposition (e.g. Gray & Zeitler 1997; Bernet *et al.* 2004; Chew *et al.* 2007). Similar paleontologically determined and radiometrically determined ages for intrusive and metamorphic rocks suggest rapid exhumation, erosion and deposition (e.g. Ghiglione *et al.* 2015; Sickmann *et al.* 2018).

The youngest valid (highly concordant) detrital zircon ages from the sandstones can be usefully compared with the paleontologically determined ages of the interbedded finer-grained sediments (Fig. 13): (1) The youngest 100% concordant ages of the Vlamborous Formation sandstones are mid-Carboniferous (320 Ma; GC14-3) and Cambrian (525 Ma; GC14-9) and, therefore, have little bearing on the paleontologically determined Late Triassic age, based mainly on the presence of the pelagic bivalve *Halobia sp.* and Radiolaria (Ealey & Knox 1975; Lapierre 1975; Robertson & Woodcock 1979; Bragin & Krylov 1996; Bragin 2007); (2) Similarly, the youngest 100% concordant age of the overlying Akamas Member sandstone (GC14-16) is Ediacaran (588 Ma), compared to the Late Jurassic-Early Cretaceous depositional age based on Radiolaria (Bragin & Krylov 1996, 1999; Bragin 2007); (3) The youngest 100% concordant age of the sandstone represented by Pareklisia Member is Ediacaran (630 Ma). Organic carbon-rich mudstones interbedded with the sandstones are tentatively dated as Early Cretaceous based on sporomorphs (Robertson 1977). Also, the clay-rich matrix of the Moni Melange has been dated as Late Cretaceous using Radiolaria (Urquhart & Banner 1994); (4) In marked contrast, the Kiparisso Vouno (Alevkaya Tepe) Member in the Kyrenia Range contains a youngest acceptable (*c.* 98% concordant) detrital zircon age of 87 Ma (Coniacian) and 95 Ma (Cenomanian). This unit is dated as Maastrichtian based on planktic foraminifera within interbedded pelagic limestones (Baroz 1979; Robertson *et al.* 2012*b*). Detrital zircons, of inferred igneous origin, crystallised, eroded and were deposited, all during Late Cretaceous time, indicating a rapid succession of tectonic-magmatic events; (5) The 100% youngest concordant age of the Kalograia-Ardana (Bahçeli–Ardahan) Formation is Middle Eocene (45 Ma). Planktic foraminifera from hemipelagic marl in the lower to mid parts of the succession indicate a similar, Middle Eocene age (Baroz 1979; Robertson *et al.* 2014), showing that magmatic cooling, exhumation, erosion and deposition again all took place rapidly; (6) For the Davlos (Kaplıca) Formation, the 100% youngest

concordant detrital zircon ages are Campanian (74 Ma). Tortonian (*c.* 10 Ma) and Serravallian (*c.* 12 Ma) zircons have 77% and 120% concordance levels, respectively. The depositional age of this formation is Tortonian based mainly on planktic foraminifera (Baroz 1979); and (7) The Mia Milia (Dağyolu) Formation is dated as Burdigalian-Tortonian based on combined planktic foraminifera and nannofossil dating (Baroz 1979; Hakyemez *et al.* 2000; McCay *et al.* 2013).

Summarising, there is no evidence of rapid (several Ma) recycling of zircons in the Mamonia Complex sedimentary succession or in the Moni Melange detached blocks (Pareklisia Member), both of which are interpreted as parts of a rifted Mesozoic passive margin succession (e.g. Robertson 1977; Robertson & Woodcock 1979; Torley & Robertson 2018). Detrital zircons in passive margin successions generally lack syn-depositional magmatism and are therefore dominated by older detrital grains (e.g. Cawood *et al.* 2012). In contrast, detrital zircons in active margin successions commonly exhibit similar-aged magmatism, as observed for the Late Cretaceous-Miocene sandstones of the Kyrenia Range.

Zircon provenance

Late Precambrian

The Late Precambrian zircon populations can be compared to the radiometrically determined ages of the Amazonia, Baltica, Siberia, West Africa, Arabian-Nubian Shield and Saharan cratonic provinces (Fig. 14). Amazonia-derived terranes (microplates) in northern South America (e.g. Tassinari & Macambira 1999) are characterised by several-aged populations: i.e. 0.9-1.1 Ga (Tonian-Stenian) related to the Grenvillian orogeny, and also Mesoproterozoic (~1.5 Ga) and Paleoproterozoic (1.7-2.2 Ga), both related to the Rondonian orogeny (Fig. 14; Tassinari & Macambira 1999; Linnemann *et al.* 2004; Winchester *et al.* 2006; Nance *et al.* 2008; Drost *et al.* 2011). The absence of significant Mesoproterozoic and Paleoproterozoic zircon populations is inconsistent with derivation from Amazonia. Baltican provenance is characterised by an undifferentiated (continuous) age population of 900-3200 Ma, with a large gap between 550 and 750 Ma (e.g. Hartz & Torsvik 2002; Linnemann *et al.* 2004; Nance *et al.* 2008). The prominent Late Neoproterozoic zircon population in the sandstones therefore opposes a Baltican provenance (Fig. 14). The Siberia Craton can also be ruled out in view of its Late Neoproterozoic magmatic quiescence (e.g. Meert & Torsvik 2003; Sunal *et al.* 2008). The W Africa Craton is characterised by several orogenic events resulting in zircon groupings at 500-750 Ma (Pan-African orogeny; Liégeois *et al.* 1994), 2.0-2.2 Ga (Eburnean orogeny; Abouchami *et al.* 1990; Liégeois *et al.* 1994), ~2.7 Ga (Liberian orogeny; Hurley *et al.* 1971) and 3.1-3.3 Ga (Leonian orogeny; Beckinsale *et al.* 1980; Linnemann *et al.* 2004). The prominent

Tonian-Stenian zircon population in the sandstones (Fig. 14) contrasts with the known 0.8-1.7 Ga magmatic quiescence in the W Africa Craton (e.g. Liégeois *et al.* 1994).

The dominant Neoproterozoic zircon populations are, instead, compatible with a NE Africa/Arabian-Nubian Shield origin. Predominant Neoproterozoic zircon populations in NE Africa and the Arabian-Nubian Shield (Avigad *et al.* 2003; Kolodner *et al.* 2006; Drost *et al.* 2011) group at 550-650 Ma, reflecting voluminous plutonic and volcanic rocks of this age within this region (e.g. Bentor 1985; Stern 1994). Subordinate pre-Neoproterozoic zircons populations of Tonian-Stenian, 1.65-1.85 Ga and *c.* 2.5 Ga are consistent with derivation from central Africa (Cahen *et al.* 1984), southeast Africa (Kröner *et al.* 2001), the Saharan Metacraton (Abdelsalam *et al.* 2002), and/or the Afif terrane of southeast Saudi Arabia (Stacey & Hedge 1984) (Fig. 2). The corresponding Pre-Neoproterozoic zircons in the Late Triassic sandstones scatter around a comparable time span (Fig. 14), although without significant zircon populations. In the Saharan Metacraton, zircon ages in the basement ranges from 1.65-2.7 Ga, with a further orogenic event around 1.0 Ga (Abdelsalam *et al.* 2002; Linnemann *et al.* 2004) (Fig. 14). The absence of significant Paleoproterozoic zircon populations in the sandstones opposes a Saharan Metacraton origin. However, Cambrian and Ordovician sandstones from Jordan, peripheral to the Arabian-Nubian Shield, have similar Precambrian-aged zircon populations to the samples studied (Kolodner *et al.* 2006) (Figs. 2, 14).

The zircon age data indicate an ultimate origin related to Gondwana. However, during Late Permian-early Mesozoic time, fragments of Gondwana rifted and drifted northwards to open the Southern Neotethys (Şengör & Yılmaz 1981; Robertson & Dixon 1984; Stampfli & Borel 2002; Göncüoğlu *et al.* 2003). Consistent with this interpretation, Gondwana-derived zircons exist in the Taurides to the north of Cyprus (e.g. Ustaömer *et al.* 2012, 2018; Zlatkin *et al.* 2013; Abbo *et al.* 2015). The occurrence of Gondwana-derived zircons in both the Vlamborous Formation and the Pakeklisia Member sandstones cannot therefore be used to indicate the paleogeographic source during the Late Triassic and Early Cretaceous when these lithologies accumulated. Sedimentological evidence has, however, established close similarities between the sedimentary and volcanic rocks of the Ayios Photios Group (Mamonia Complex) and the Isparta Angle area of SW Turkey (Taurides) suggesting derivation from the north or northwest of the present outcrops in Cyprus (Robertson, 2000; Torley & Robertson, 2018) (Fig. 2). Specifically, the Lower Paleozoic siliciclastic cover of the Menderes Massif in western Turkey (Zlatkin *et al.* 2013) and the Paleozoic to Triassic siliciclastic rocks of the Karacahisar dome in the Taurides (Abbo *et al.* 2015) both contain Gondwana-derived zircons. The zircon grains in the Triassic and Early Cretaceous Cyprus sandstones are likely to have been recycled from Paleozoic sedimentary successions of southern and central Turkey (Fig. 15).

Paleozoic

For time periods prior to the Permo-Triassic rifting of the Southern Neotethys, any zircons with Gondwanan signatures, in principle, could have been derived directly from the NE Africa/Arabian-Nubian Shield, or from Turkey to the north. Paleozoic zircons (<540 Ma) constitute a trace to minor fraction of the sandstones analysed, except for the Late Miocene sandstone of the Kyrenia Range (although this could be an artefact of limited analysis). Although poorly concordant, the oldest of these zircon populations (Ediacaran-Early Cambrian) is similar to that of granitic arc rocks in the Bitlis Massif of southeast Turkey (Usta ömer P. A. *et al.* 2009, 2012*a*) (Fig. 2). Prominent zircon populations of Early Cambrian, Late Neoproterozoic and Tonian-Stenian ages in this area are again suggestive of an Arabian-Nubian Shield origin (Usta ömer P. A. *et al.* 2009, 2012*a*). The prolonged Ediacaran-Early Cambrian age is likely to record Andean-type magmatism along the northern margin of Gondwana in the Eastern Mediterranean region (Usta ömer P. A. *et al.* 2009). Zircons of Early Cambrian (~500-550 Ma) age could represent either circum-Gondwana convergent magmatism or late Pan-African amalgamation of the Gondwana continent.

The second-oldest Paleozoic zircon population includes detrital zircons of Ordovician-Carboniferous age with peaks during Middle Ordovician, Late Silurian and mid-Carboniferous times. Ordovician magmatism (specifically Middle Ordovician) is known in the Armutlu Peninsula and also in the Tavşanlı zone (Orhaneli region), both in NW Turkey (Okay 2002; Okay *et al.* 2008*a, b*; Özbey *et al.* 2013) (Fig. 2). The Silurian magmatism implied by the zircon ages could be represented by the known bimodal volcanism along the northern margin of the Tauride-Anatolide platform (Göncüoğlu & Kozlu 2000; Eren *et al.* 2004). Only minor local volcanic activity (pre-Late Permian) is known in the Antalya (SW Taurides) and Feke (E Taurides) regions (Göncüoğlu & Kozlu 2000) (Fig. 2). The Carboniferous of the northern margin of the Anatolide-Tauride block (e.g. Afyon zone; Konya area) (Fig. 2) is characterised by a melange (Konya Melange) that includes terrigenous-derived siliciclastic sandstones, Late Paleozoic shallow-water carbonates, Silurian-Devonian black chert and Carboniferous-aged subduction-influenced volcanic rocks (Robertson & Usta ömer 2009*a, b*, 2011). Carboniferous granites were recently reported from the Afyon zone elsewhere (Candan *et al.* 2016). Carboniferous volcanic rocks are also documented in the Sultan Dağ area of the Tauride platform (Göncüoğlu *et al.* 2007; Mackintosh & Robertson 2012) (Fig. 2). In one hypothesis, all of the above units are related to magmatism and tectonic accretion along northern margin of the Anatolide-Tauride continental block that rifted from Gondwana during Late Permian-Late Triassic time (Göncüoğlu *et al.* 2003; Robertson & Usta ömer 2009*a*). In an alternative hypothesis (Stampfli & Borel, 2002), zircons associated with the Anatolide crustal block (e.g. Afyon zone; Konya area) were

partly derived from the Pontides farther north, requiring Gondwana-derived crust to have accreted to Eurasia during the Paleozoic.

Carboniferous magmatism is also well-documented in the Pontides of northern Turkey. For some authors, this Carboniferous magmatism was related to northward subduction to create a south-Laurasian continental margin magmatic arc during the Variscan orogeny (Stampfli & Borel 2002; Topuz *et al.* 2010; Usta ömer P. A. *et al.* 2012*b*; Usta ömer *et al.* 2013; Okay & Nikishin 2015). Alternatively, others infer southward subduction and formation of a major continental margin arc (Sakarya crustal unit) adjacent to the northern margin of Gondwana (Şengör & Yılmaz 1981; Yılmaz *et al.* 1997; Göncüoğlu *et al.* 2000).

Zircons with ages indicative of a north-Gondwana derivation have also been reported from Paleozoic sandstones of the Pontides, including the pre-Lower Carboniferous meta-sedimentary schists of the Central Sakarya Basement, western Pontides (Usta ömer P. A. *et al.* 2012*b*), the Mid-Devonian and early Carboniferous Karadağ paragneiss and the Ordovician to early Carboniferous Narlık schist, eastern Pontides (Usta ömer *et al.* 2013). These Pontide meta-sandstones are interpreted to have been derived from crustal units that rifted from Gondwana, drifted across Paleotethys and accreted to Eurasia during the Paleozoic, prior to the rifting of the Southern Neotethys during Permo-Triassic time (e.g. Usta ömer *et al.* 2013). However, some authors reposition these crustal units adjacent to the northern margin of the Anatolide crustal block, as noted above (Şengör & Yılmaz 1981; Yılmaz *et al.* 1997; Göncüoğlu *et al.* 2000). In the absence of agreement on the regional tectonic setting, the source of the Carboniferous magmatism represented in the Cyprus sandstones analysed remains an open question (see Usta ömer *et al.* 2014, 2016*a*; Usta ömer P. A. *et al.* 2014).

Mesozoic

Extensive Triassic rift-related magmatism is documented from the Mamonia Complex (Dhiarizos Group), SW Cyprus (Lapierre 1975; Robertson & Woodcock 1979; Chan *et al.* 2008) and in the Antalya Complex (Gödene Zone), SW Turkey (Juteau 1975; Robertson & Woodcock 1981*a*, *b*, *c*). Triassic, rift-related volcanic rocks (mostly evolved) also occur widely in the more northerly-derived Beyşehir-Hoyran-Hadim Nappes, central Taurides (Fig. 2) (Özgül 1984; Andrew & Robertson 2002). Stratigraphic evidence from the central Taurides (e.g. Hadim and Bolkar nappes) suggests that rifting began during the Late Permian (Mackintosh & Robertson 2012). The rare Permian zircons within the Cyprus sandstones are therefore interpreted to reflect rift-related magmatism in southern Turkey, although magmatic rocks of this age are poorly known. Only the Eocene sandstones of the Kyrenia Range were observed to contain Triassic zircons during this study (Fig. 11d). The Triassic igneous rocks in W Cyprus (Dhiarizos Group; Mamonia Complex) formed in a relatively distal (oceanic)

setting and were therefore unavailable as a source for more proximal rift and passive margin sediments (i.e. Ayios Photios Group; Mamonia Complex). In contrast, the Eocene sandstones of the Kyrenia Range accumulated in a foredeep setting, derived from deformed lithologies, including Triassic rift-related sandstones, as widely exposed in the Taurides farther north (e.g. Antalya Complex) (Robertson & Woodcock 1984).

Late Cretaceous (71-95 Ma) zircons characterise the Late Cretaceous-Neogene sandstones of the Kyrenia Range. Occasional Turonian-Coniacian (86-94 Ma) zircon grains are present, with Th/U ratios (>0.1) and typical zoning structures of igneous rocks (Rubatto 2002; Corfu *et al.* 2003; Teipel *et al.* 2004). These sandstones contain abundant, well-mixed detritus that, taken together, includes serpentinite, variably recrystallised radiolarian chert/shale and minor amounts of basalt/diabase, which are indicative of an ophiolite-related origin (McCay & Robertson 2012; Robertson *et al.* 2012*b*, 2014). Supra-subduction zone (SSZ)-type ophiolites that overlie the Tauride platform in southern Turkey (e.g. Antalya, Beyşehir and Mersin areas; Fig. 2) have yielded similar Late Cretaceous radiometric ages (~85-95 Ma) (e.g. Parlak & Delaloye 1999; Çelik *et al.* 2006; Karaoğlan *et al.* 2012, 2013*a*). The Mersin ophiolite and related accretionary melange (Parlak & Robertson 2004; Robertson *et al.* 2012*a*) are the nearest appropriate units to have supplied the Late Cretaceous zircons within the Late Cretaceous-Neogene sandstones of the Kyrenia Range, although the exact source remains uncertain.

The abundant Santonian-Campanian-aged zircons (73-86 Ma) in the Kyrenia Range sandstones (e.g. Davlos (Kaplıca) and the Mia Milia (Dağyolu) Formations) are likely to have a source area to the east, as inferred from generally westward paleocurrents in these sandstones (Weiler 1970; McCay & Robertson 2012). There are two main *c.* NE-SW trending belts of ophiolitic rocks of Late Cretaceous age (*c.* 84-92 Ma) in SE Turkey and N Syria. The southerly one is characterised by a chain of ophiolites and related accretionary melange. These include the Baer-Bassit ophiolite (Al-Riyami *et al.* 2002) in northern Syria, the Hatay ophiolite (Boulton & Robertson 2007; Karaoğlan *et al.* 2012, 2013*a*), the Amanos ophiolite (Duman *et al.* 2017) and the Koçali ophiolite (Robertson *et al.* 2016), which are located in southern Turkey or northernmost Syria (Fig. 2). Some areas of SE Turkey (e.g. Göksun–Afşin (Kahramanmaraş), Doğanşehir (Malatya) and Baskil (Elazığ) regions) include subduction-related granitic rocks (77-85 Ma) (e.g. Aktaş & Robertson 1990; Parlak 2006; Rızaoğlu *et al.* 2006, 2009; Robertson *et al.* 2007) (Fig. 2). The nearest appropriate source is the combined Hatay and Amanos ophiolites. In summary, any of the above Late Cretaceous ophiolitic or arc-related igneous rocks of SE Turkey are potential sources of the Santonian-Campanian zircons in the Kyrenia Range.

Cenozoic

Traces of Paleocene, Eocene and Miocene-aged zircons occur in the Eocene and Miocene sandstones of the Kyrenia Range. Convergence of the African and Eurasian plates took place during Late Cretaceous-Cenozoic time, related to northward subduction of the Southern Neotethys (Livermore & Smith 1985; Savostin *et al.* 1986; Barrier *et al.* 2018). In the Kyrenia Range, Maastrichtian-Early Eocene within-plate-type basalts (with a local subduction influence) are interpreted to represent an extensional setting related to on-going development of the inferred South Neotethyan active continental margin (Robertson & Woodcock 1986; Huang *et al.* 2007; Chen 2018).

The Paleogene volcanism represented by the Ayios Nikolaos (Yamaçköy) Formation in the Kyrenia Range rarely extended into the Early Eocene, based on planktic foraminiferal dating of interbedded pelagic carbonates in the eastern range (Robertson *et al.* 2012*b*). The Early Eocene zircons in the overlying sandstone turbidites (Kalograia-Ardana (Bahçeli–Ardahan) Formation) might therefore have been derived from local coeval volcanism in the Kyrenia Range. However, the sedimentology and petrography of these sandstones point to a more distal source, which included abundant ophiolitic detritus (especially serpentinite and boninite) and also radiolarian chert (Robertson *et al.* 2014). These Eocene sediments accumulated in a foredeep during continued development of the South-Neotethyan active continental margin, with sediment supply mainly from the north (Robertson *et al.* 2014). Northward subduction of Southern Neotethys (Aktaş & Robertson 1990; Elmas & Yılmaz 2003; Robertson *et al.* 2012*b*) gave rise to widespread subduction-related, andesitic volcanism (e.g. Helete Formation) in SE Turkey, as documented from a thrust belt overlying the northern margin of the Arabian platform (Robertson *et al.* 2006; Karaoğlan *et al.* 2013*b*; Nurlu *et al.* 2016). Paleocene volcanogenic rocks are also exposed farther north, along the northern margin of the Anatolide-Tauride, specifically in the Ulukışla Basin (Clark & Robertson 2002) (Fig. 2), although this remote area is a less likely source.

Late Oligocene zircons occur in the Miocene sandstone of the Kyrenia Range. Oligocene volcanics (Gövelek unit) occur in the Lake Van area, SE Turkey (Robertson *et al.* 2006; Oyan 2018) (Fig. 2), although this is *c.* 900 km to the east of Cyprus, suggesting that a more local source remains to be identified.

Miocene zircons are likely to have been supplied by local reworking of tuffaceous layers within the nearby Panagra (Geçitköy) Formation (*c.* 19.8 Ma) in the Kyrenia Range (Baroz 1979; Chen 2018). Accumulation as air-fall tuff is supported by the relatively euhedral shape of the zircons. The probable source of the tuff was Early Miocene rhyolitic and tuffaceous volcanism to the northwest, within the Isparta Angle (SW Turkey) (Yağmurlu *et al.* 1997; Dilek & Altunkaynak 2010; Seghedi & Helvacı 2016) (Fig. 2). Miocene volcanics of the Amanos Mountain to the northeast are unlikely to

have been a source because these are mainly basic to intermediate-composition lava flows rather than tuffs (Robertson *et al.* 2006; Duman *et al.* 2017) (Fig. 2). Miocene collision-related volcanism occurs in eastern Turkey (i.e. Eastern Anatolian Volcanic Province; Innocenti *et al.* 1982; Pearce *et al.* 1990), but as noted above this area is too far away to represent a realistic source.

Implications for tectonic reconstructions

The dominance of Ediacaran-Cryogenian and Tonian-Stenian detrital zircon populations is indicative of ultimate derivation from the NE Africa/Arabian-Nubian Shield (Figs. 15-16; see above). During the Late Permian-Early Jurassic the Tauride continental units rifted from North Africa giving rise to several microcontinental units to the north of Cyprus, as noted above (e.g. Robertson & Woodcock 1984; Göncüoğlu *et al.* 2003; Garfunkel 2004; Robertson *et al.* 2009; Ustaömer *et al.* 2016*b*; Barrier *et al.* 2018). By the time that the first MORB (mid-ocean ridge basalt) appeared in western Cyprus, represented by the Dhiarizos Group (Mamonia Complex) (Fig. 4), any Precambrian zircons could have either a southerly source (NE Africa/Arabian-Nubian Shield) or a northerly source (rifted away Gondawan crust) (Fig. 15).

The facies and age of the sedimentary and igneous rocks of the Mamonia Complex are markedly similar to those of the Antalya Complex within the Isparta Angle (SW Taurides) to the northwest (Robertson & Woodcock 1981*a, b, c*) (Fig. 2). The western limb of the Isparta Angle, today continues southwards offshore as the submarine Anaximander Mountains (Zitter *et al.* 2003). This crust could represent the hinterland of the Mamonia Complex during the Mesozoic (Clube & Robertson, 1986; Torley & Robertson 2018). A related study of Triassic sandstones associated with the Tauride continental block (Ustaömer *et al.* 2014, 2016*a*, 2018; Ustaömer P. A. *et al.* 2014) identifies possible source areas within Paleozoic shallow-marine shelf successions, including Devonian-Triassic quartz-rich sandstones of the Hadim and Bolkar Nappes (central Taurides) (Özgül 1984; Mackintosh & Robertson 2012) (Fig. 2). These lithologies are interpreted to have been derived from local basement highs of Late Precambrian age (Göncüoğlu *et al.* 2003; Mackintosh & Robertson 2012), notably the Sandıklı Basement Complex (Fig. 2). The lithologies include Late Precambrian-Cambrian low-grade meta-sedimentary rocks and siliceous volcanic rocks (Gürsu *et al.* 2004; Ghienne *et al.* 2010). A northerly derivation is inferred for the Late Triassic and Early Cretaceous sandstones of the Mamonia Complex after rifting of the Southern Neotethys, despite their ultimate derivation from Gondwana (Figs. 15, 16). The Ediacaran-Cryogenian and Tonian-Stenian zircon populations in the sandstones of the Eocene Kalograia-Ardana (Bahçeli–Ardahan) Formation, the Late Miocene Davlos (Kaplıca) Formation and the Middle to Late Miocene Mia Milia (Dağyolu) Formation of the Kyrenia Range are also likely to have been recycled from Paleozoic siliciclastic

617 sedimentary rocks within Anatolia, with initial derivation (prior to Triassic rifting) from the NE
618 Africa/Arabian-Nubian Shield of N Gondwana.

619 During Campanian-Early Miocene, northward subduction was active along the northerly
620 continental margin of the Southern Neotethys (Aktaş & Robertson 1984; Robertson & Dixon 1984;
621 Yılmaz 1993; Yılmaz *et al.* 1997; Robertson *et al.* 2012*b*; Barrier *et al.* 2018) (Fig. 16). Large
622 volumes of clastic sediments accumulated in an active margin (foredeep) setting along the southern
623 margin of the Tauride continental crust in Cyprus, including the Maastrichtian Kiparisso Vouno
624 (Alevkaya Tepe) Member in the Kyrenia Range (Fig. 16b). The overlying Maastrichtian-Early
625 Eocene basaltic rocks erupted in an extensional active margin setting (Pearce 1975; Robertson &
626 Woodcock 1986; Huang *et al.* 2007; Chen 2018). The clastic detritus was probably derived from by-
627 then emplaced ophiolite and arc-related units to the north (e.g. Mersin ophiolite and melange; Parlak
628 & Robertson 2004; Robertson *et al.* 2012*b*), where suitable source rocks are exposed.

629 The Taurides were affected by regional-scale southward thrusting during Early-Middle Eocene
630 time, driven by suturing of the İzmir–Ankara–Erzincan ocean farther north (Şengör & Yılmaz 1981;
631 Özgül 1984; Okay *et al.* 2001; Mackintosh & Robertson 2013). In addition, the Arabian platform
632 was also deformed to the northeast of Cyprus, notably in the Amanos Mountains (Duman *et al.* 2017).
633 The pre-existing active continental margin in the Kyrenia Range was reactivated to create a regional
634 foredeep that filled with Eocene gravity deposits, including sedimentary melange, as represented by
635 the Kalaograia–Ardana (Bahçeli–Ardahan) Formation (Robertson *et al.* 2014) (Fig. 16c).

636 Limited paleocurrent evidence (McCay & Robertson 2012; Robertson *et al.* 2014) suggests a
637 general south-Tauride source for the basal, Late Eocene interval of the Bellapais (Beylerbey)
638 Formation, similar to the inferred provenance of underlying Maastrichtian and Eocene sandstones. In
639 contrast, westerly-directed paleocurrents evidence suggests SE Turkey as the main source of the
640 Oligocene part of the Bellapais (Beylerbeyi) Formation, upwards to and including the Late Miocene
641 Mia Milia (Dağyolu) Formation (McCay & Robertson 2012). In SE Turkey, a wide range of
642 lithologies were emplaced southwards onto the Arabian platform during Oligocene-Early Miocene
643 time, including Mesozoic platform carbonates, greenschist facies metamorphic units, Late
644 Cretaceous ophiolites, Mesozoic-Early Cenozoic sedimentary and volcanic units, and both Late
645 Cretaceous and Eocene arc-related magmatic rocks (Aktaş & Robertson 1984; Perinçek & Kozlu
646 1984; Yılmaz 1993; Robertson *et al.* 2006; Bağci *et al.* 2008; Karaoğlan *et al.* 2016). During and
647 after this emplacement, the thrust stack supplied clastic sediment (Lice Formation) to the Neogene
648 foreland basin to the south, extending westwards into the Oligocene-Miocene foredeep represented
649 by the Kyrenia Range thrust belt farther west (McCay & Robertson 2012, 2013) (Fig. 16d). Collision

between the Kyrenia Range and the Troodos Massif was achieved by Late Miocene-Early Pliocene time although strike slip offset continues along the intervening Ovgos (Dar Dere) Fault.

Conclusions

- Late Triassic sandstones of the Mesozoic passive margin, represented by the Ayios Photios Group (Mamonia Complex) in W Cyprus are dominated by Ediacaran-Cryogenian (*c.* 540-720 Ma) and Tonian-Stenian-aged (*c.* 750-1100 Ma) zircon populations, indicating an ultimate north-Gondwana origin (NE Africa/Arabian-Nubian Shield). Based on facies comparisons, the direct source lithologies are likely to be Paleozoic siliciclastic shelf successions in the Taurides (to the north) that were detached from Gondwana as part of a microcontinent during Late Permian-Early Jurassic rifting of the Southern Neotethys.
- The Late Jurassic-Early Cretaceous deep-water slope sandstones of the Late Jurassic-Early Cretaceous Ayios Photios Group have similar zircon populations to those of the underlying Late Triassic sandstones, as do the shallow-marine sandstones of the Early Cretaceous Pareklisia Member (detached blocks) of the Moni Melange (S Cyprus), suggesting a similar provenance.
- Late Cretaceous (Maastrichtian) and Eocene sandstones from successions in the Kyrenia Range are also dominated by Edicarian-Cryogenian and Tonian-Stenian zircons, again indicating an ultimate northern Gondwana source prior to rifting of continental crust from Gondwana to open the Southern Neotethys. These zircons were probably derived from Tauride units to the north during and after Late Cretaceous regional deformation related to the initial stages of closure of the Southern Neotethys.
- A minor fraction of Late Cretaceous zircons in the Maastrichtian and Eocene sandstones of the Kyrenia Range was derived from a nearly contemporaneous continental margin arc and/or ophiolite-related units that were probably located within the Taurides to the north.
- The new detrital zircon age data confirm that the sandstones of the Mamonia Complex (W Cyprus) and the Moni Melange (S Cyprus) relate to a Mesozoic rifted passive margin, whereas the Late Cretaceous-Miocene sandstones of the Kyrenia Range (N Cyprus) represent active margin and collisional settings.

Acknowledgements

We particularly thank Dr. Richard Hinton, Dr. Steffen Kutterolf and Prof. Dick Kroon for scientific discussion. Dr. Linda Kirstein and Prof. Simon Harley advised on zircon separation. Mr. Mike Hall prepared the polished blocks for zircon analysis. In addition, the manuscript has benefited from the

683 detailed and constructive comments of Solomon Buckman, an anonymous reviewer and the editor,
684 Prof. Peter Clift.
685
686 **Funding**
687 The first author gratefully acknowledges the receipt of a joint studentship of the Principal's Career
688 Development PhD Scholarship and Edinburgh Global Research Scholarship. The authors are grateful
689 for financial support from the Natural Environment Research Council-Ion Microprobe Facility (to A.
690 H. F. Robertson) to carry out SIMS U-Pb dating of detrital zircons.
691
692

693 **References**
694

695 Abbo, A., Avigad, D., Gerdes, A. & Güngör, T. 2015. Cadomian basement and Paleozoic to Triassic
696 siliciclastics of the Taurides (Karacahisar dome, south-central Turkey): Paleogeographic
697 constraints from U-Pb-Hf in zircons. *Lithos*, **227**, 122-139.

698 Abdelsalam, M.G., Liégeois, J.-P. & Stern, R.J. 2002. The saharan metacraton. *Journal of African*
699 *Earth Sciences*, **34**, 119-136.

700 Abouchami, W., Boher, M., Michard, A. & Albarede, F. 1990. A major 2.1 Ga event of mafic
701 magmatism in West Africa: an early stage of crustal accretion. *Journal of Geophysical Research:*
702 *Solid Earth*, **95**, 17605-17629.

703 Aktaş, G. & Robertson, A.H.F. 1984. The Maden Complex, SE Turkey: evolution of a Neotethyan
704 active margin. *In*: Dixon, J.E. & Robertson, A.H.F. (eds) *The Geological Evolution of the*
705 *Eastern Mediterranean*. Geological Society, London, Special Publications, **17**, 375-402.

706 Aktaş, G. & Robertson, A.H.F. 1990. Tectonic evolution of the Tethys suture zone in SE Turkey:
707 evidence from the petrology and geochemistry of Late Cretaceous and Middle Eocene
708 extrusives. *In*: Malpas, J., Moores, E. M., Panayiotou, A. & Xenophontos, C. (eds) *Ophiolites-*
709 *Oceanic Crustal Analogues. Proceedings of the International Symposium 'Troodos 1987'*.
710 Geological Survey Department, Nicosia, Cyprus, 311-329.

711 Al-Riyami, K., Robertson, A., Dixon, J. & Xenophontos, C. 2002. Origin and emplacement of the
712 Late Cretaceous Baer-Bassit ophiolite and its metamorphic sole in NW Syria. *Lithos*, **65**, 225-
713 260.

714 Andersen, T. 2005. Detrital zircons as tracers of sedimentary provenance: limiting conditions from
715 statistics and numerical simulation. *Chemical Geology*, **216**, 249-270.

716 Andrew, T. & Robertson, A.H.F. 2002. The Beyşehir-Hoyran-Hadim Nappes: genesis and
717 emplacement of Mesozoic marginal and oceanic units of the northern Neotethys in southern
718 Turkey. *Journal of the Geological Society*, **159**, 529-543.

719 Avigad, D., Kolodner, K., McWilliams, M., Persing, H. & Weissbrod, T. 2003. Origin of northern
720 Gondwana Cambrian sandstone revealed by detrital zircon SHRIMP dating. *Geology*, **31**, 227-
721 230.

722 Avigad, D., Weissbrod, T., Gerdes, A., Zlatkin, O., Ireland, T.R. & Morag, N. 2015. The detrital
723 zircon U-Pb-Hf fingerprint of the northern Arabian-Nubian Shield as reflected by a Late
724 Ediacaran arkosic wedge (Zenifim Formation; subsurface Israel). *Precambrian Research*, **266**,
725 1-11.

726 Bağci, U., Parlak, O. & Höck, V. 2008. Geochemistry and tectonic environment of diverse magma
727 generations forming the crustal units of the Kızıldağ (Hatay) ophiolite, Southern Turkey.
728 *Turkish Journal of Earth Sciences*, **17**, 43-71.

729 Baroz, F. 1979. *Etude Géologique Dans Le Pentadaktylos et La Mesaoria (Chypre Septentrionale)*.
730 PhD thesis, Université de Nancy.

731 Barrier, E., Vrielynck, B., Brouillet, J.F. & Brunet, M.F. 2018. *Paleotectonic Reconstruction of the*
732 *Central Tethyan Realm. Tectonono-Sedimentary-Palinspastic Maps from Late Permian to*
733 *Pliocene.* CCGM/CGMW, Paris, Atlas of 20 maps (scale: 1/15000000).

734 Beckinsale, R.D., Gale, N.H., Pankhurst, R.J., Macfarlane, A., Crow, M.J., Arthurs, J.W. &
735 Wilkinson, A.F. 1980. Discordant Rb-Sr and Pb-Pb whole rock isochron ages for the Archaean
736 basement of Sierra Leone. *Precambrian Research*, **13**, 63-76.

737 Bentor, Y.K. 1985. The crustal evolution of the Arabo-Nubian Massif with special reference to the
738 Sinai Peninsula. *Precambrian Research*, **28**, 1-74.

739 Bernet, M., Brandon, M.T., Garver, J.I. & Molitor, B.R. 2004. Fundamentals of detrital zircon
740 fission-track analysis for provenance and exhumation studies with examples from the European
741 Alps. In: Bernet, M. & Spiegel, C. (eds) *Detrital Thermochronology-Provenance Analysis,*
742 *Exhumation, and Landscape Evolution of Mountain Belts.* Geological Society of America,
743 Special Papers, **378**, 25-94.

744 Boulton, S.J. & Robertson, A.H.F. 2007. The Miocene of the Hatay area, S Turkey: Transition from
745 the Arabian passive margin to an underfilled foreland basin related to closure of the Southern
746 Neotethys Ocean. *Sedimentary Geology*, **198**, 93-124.

747 Bozkurt, E., Park, R.G. & Winchester, J.A. 1993. Evidence against the core/cover interpretation of
748 the southern sector of the Menderes Massif, west Turkey. *Terra Nova*, **5**, 445-451.

749 Bragin, N.Y. 2007. Late Triassic radiolarians of southern Cyprus. *Paleontological Journal*, **41**, 951-
750 1029.

751 Bragin, N.Y. & Krylov, K.A. 1996. Stratigraphy and lithology of the Upper Triassic deposits of
752 southwestern Cyprus (Vlambouros Formation). *Stratigraphy and Geological Correlation*, **4**,
753 132-140.

754 Bragin, N.Y. & Krylov, K.A. 1999. Stratigraphy and formation conditions of the Jurassic siliceous
755 and terrigenous deposits in Southwestern Cyprus. *Stratigraphy and Geological Correlation*, **7**,
756 333-342.

757 Buckman, S., Aitchison, J.C., Nutman, A.P., Bennett, V.C., Saktura, W.M., Walsh, J.M.J.,
758 Kachovich, S. & Hidaka, H. 2018. The Spongtang Massif in Ladakh, NW Himalaya: An Early
759 Cretaceous record of spontaneous, intra-oceanic subduction initiation in the Neotethys.
760 *Gondwana Research*, **63**, 226-249.

761 Cahen, L., Snelling, N.J., Delhal, J. & Vail, J.R. 1984. *The Geochronology and Evolution of Africa*.
762 Clarendon Press, Oxford.

763 Candan, O., Akal, C., Koralay, O.E., Okay, A.I., Oberhänsli, R., Prelević, D. & Mertz-Kraus, R.
764 2016. Carboniferous granites on the northern margin of Gondwana, Anatolide-Tauride Block,
765 Turkey - Evidence for southward subduction of Paleotethys. *Tectonophysics*, **683**, 349-366.

766 Cawood, P.A., Hawkesworth, C.J. & Dhuime, B. 2012. Detrital zircon record and tectonic setting.
767 *Geology*, **40**, 875-878.

768 Çelik, Ö.F., Delaloye, M. & Feraud, G. 2006. Precise ^{40}Ar-^{39}Ar ages from the metamorphic sole
769 rocks of the Tauride Belt Ophiolites, southern Turkey: implications for the rapid cooling history.
770 *Geological Magazine*, **143**, 213-227.

771 Chan, G.H.-N., Malpas, J., Xenophontos, C. & Lo, C.-H. 2008. Magmatism associated with
772 Gondwanaland rifting and Neo-Tethyan oceanic basin development: evidence from the
773 Mamonia Complex, SW Cyprus. *Journal of the Geological Society*, **165**, 699-709.

774 Chen, G. 2018. *Provenance-Related Studies of Triassic-Miocene Tethyan Sedimentary and Igneous*
775 *Rocks from Cyprus*. PhD thesis, University of Edinburgh, UK.

776 Chew, D.M., Schaltegger, U., Košler, J., Whitehouse, M.J., Gutjahr, M., Spikings, R.A. & Mišković,
777 A. 2007. U-Pb geochronologic evidence for the evolution of the Gondwanan margin of the
778 north-central Andes. *Bulletin of the Geological Society of America*, **119**, 697-711.

779 Clark, M. & Robertson, A. 2002. The role of the Early Tertiary Ulukisla Basin, southern Turkey, in

780 suturing of the Mesozoic Tethys ocean. *Journal of the Geological Society*, **159**, 673-690.

781 Clube, T.M.M. & Robertson, A.H.F. 1986. The palaeorotation of the Troodos microplate, Cyprus, in
782 the Late Mesozoic-Early Cenozoic plate tectonic framework of the Eastern Mediterranean.
783 *Surveys in Geophysics*, **8**, 375-437.

784 Cohen, K.M., Finney, S.C., Gibbard, P.L. & Fan, J. 2018. The ICS international Chronostratigraphic
785 Chart. *Episodes*, **36**, 199-204.

786 Corfu, F., Hanchar, J.M., Hoskin, P.W.O. & Kinny, P. 2003. Atlas of zircon textures. *Reviews in*
787 *Mineralogy and Geochemistry*, **53**, 469-500.

788 Dilek, Y. & Altunkaynak, Ş. 2010. Geochemistry of Neogene-Quaternary alkaline volcanism in
789 western Anatolia, Turkey, and implications for the Aegean mantle. *International Geology*
790 *Review*, **52**, 631-655.

791 Drost, K., Gerdes, A., Jeffries, T., Linnemann, U. & Storey, C. 2011. Provenance of Neoproterozoic
792 and early Paleozoic siliciclastic rocks of the Teplá-Barrandian unit (Bohemian Massif):
793 Evidence from U-Pb detrital zircon ages. *Gondwana Research*, **19**, 213-231.

794 Ducloz, C. 1972. *The Geology of the Bellapais-Kythrea Area of the Central Kyrenia Range*. Bulletin
795 of the Geological Survey Department, **6,** Nicosia, Cyprus.

796 Duman, T.Y., Robertson, A.H.F., Elmacı, H. & Kara, M. 2017. Palaeozoic-Recent geological
797 development and uplift of the Amanos Mountains (S Turkey) in the critically located
798 northwesternmost corner of the Arabian continent. *Geodinamica Acta*, **29**, 103-138.

799 Ealey, P.J. & Knox, G.J. 1975. The pre-Tertiary rocks of SW Cyprus. *Geologie en Mijnbouw*, **54**, 85-
800 100.

801 Elmas, A. & Yılmaz, Y. 2003. Development of an oblique subduction zone-tectonic evolution of the
802 Tethys suture zone in southeast Turkey. *International Geology Review*, **45**, 827-840.

803 Eren, Y. şar, Kurt, H., Rosselet, F. & Stampfli, G.M. 2004. Palaeozoic deformation and magmatism
804 in the northern area of the Anatolide block (Konya), witness of the Palaeotethys active margin.
805 *Eclogae Geologicae Helvetiae*, **97**, 293-306.

806 Fedo, C.M., Sircombe, K.N. & Rainbird, R.H. 2003. Detrital zircon analysis of the sedimentary
807 record. *Reviews in Mineralogy and Geochemistry*, **53**, 277-303.

808 Friedl, G., Finger, F., Paquette, J.-L., von Quadt, A., McNaughton, N.J. & Fletcher, I.R. 2004. Pre-
809 Variscan geological events in the Austrian part of the Bohemian Massif deduced from U-Pb
810 zircon ages. *International Journal of Earth Sciences*, **93**, 802-823.

811 Garfunkel, Z. 2004. Origin of the Eastern Mediterranean basin: A reevaluation. *Tectonophysics*, **391**,
812 11-34.

813 Gass, I.G. 1968. Is the Troodos Massif of Cyprus a fragment of Mesozoic ocean floor? *Nature*, **220**,
814 39-42.

815 Gass, I.G. 1990. Ophiolites and oceanic lithosphere. *In*: J. Malpas A. Panayiotou & C. Xenophontos,
816 E. M. M. (ed.) *Ophiolites: Oceanic Crustal Analogues*. Cyprus Geological Survey Department,
817 Nicosia, Cyprus, 1-12.

818 Ghienne, J.-F., Monod, O., Kozlu, H. & Dean, W.T. 2010. Cambrian-Ordovician depositional
819 sequences in the Middle East: A perspective from Turkey. *Earth-Science Reviews*, **101**, 101-146.

820 Ghiglione, M.C., Naipauer, M., Sue, C., Barberón, V., Valencia, V., Aguirre-Urreta, B. & Ramos,
821 V.A. 2015. U-Pb zircon ages from the northern Austral basin and their correlation with the
822 Early Cretaceous exhumation and volcanism of Patagonia. *Cretaceous Research*, **55**, 116-128.

823 Göncüoğlu, M.C. & Kozlu, H. 2000. Early Paleozoic evolution of the NW Gondwanaland: data from
824 southern Turkey and surrounding regions. *Gondwana Research*, **3**, 315-324.

825 Göncüoğlu, M.C., Turhan, N., Şentürk, K., Özcan, A., Uysal, Ş. & Yalınız, M.K. 2000. A
826 geotraverse across northwestern Turkey: tectonic units of the Central Sakarya region and their
827 tectonic evolution. *In:* Bozkurt, E., Winchester, J.A. & Piper, J.D.A. (eds) *Tectonics and*
828 *Magmatism in Turkey and the Surrounding Area*. Geological Society, London, Special
829 Publications, **173**, 139-161.

830 Göncüoğlu, M.C., Turhan, N. & Tekin, U.K. 2003. Evidence for the Triassic rifting and opening of
831 the Neotethyan Izmir-Ankara Ocean and discussion on the presence of Cimmerian events at the
832 northern edge of the Tauride-Anatolide Platform, Turkey. *Bolletino della Societa Geologica*
833 *Italiano, Special Volume*, **2**, 203-212.

834 Göncüoğlu, M.C., Capkinoglu, S., et al. 2007. The Mississippian in the Central and Eastern Taurides
835 (Turkey): constraints on the tectonic setting of the Tauride-Anatolide Platform. *Geologica*
836 *Carpathica*, **58**, 427.

837 Gray, M.B. & Zeitler, P.K. 1997. Comparison of clastic wedge provenance in the Appalachian
838 foreland using U/Pb ages of detrital zircons. *Tectonics*, **16**, 151-160.

839 Guiraud, R., Issawi, B. & Bosworth, W. 2001. Phanerozoic history of Egypt and surrounding areas.
840 *In*: Ziegler, P. A., Cavazza, W., Robertson, A. H. F. & Crasquin-Soleau, S. (eds) *Peri-Tethys*
841 *Mem. 6: Peri-Tethyan Rift/Wrench Basins and Passive Margins*. Museam National D'Histoire,
842 473.

843 Gürsu, S., Göncüoglu, M.C. & Bayhan, H. 2004. Geology and geochemistry of the pre-Early
844 Cambrian rocks in the Sandikli area: implications for the Pan-African evolution of NW
845 Gondwanaland. *Gondwana Research*, **7**, 923-935.

846 Hakyemez, Y., Turhan, N., Sönmez, I. & Sümengen, M. 2000. *Kuzey Kıbrıs Türk Cumhuriyeti Nin*
847 *Jeolojisi (Geology of the Turkish Republic of Northern Cyprus)*. Genel Mudurlugu Jeoloji
848 Etutleri Diaresi, Maden Tektik ve Arama, Ankara.

849 Harrison, R., Newell, W., *et al.* 2004. Tectonic framework and Late Cenozoic tectonic history of the
850 northern part of Cyprus: implications for earthquake hazards and regional tectonics. *Journal of*
851 *Asian Earth Sciences*, **23**, 191-210.

852 Hartz, E.H. & Torsvik, T.H. 2002. Baltica upside down: a new plate tectonic model for Rodinia and
853 the Iapetus Ocean. *Geology*, **30**, 255-258.

854 Huang, K., Malpas, J. & Xenophontos, C. 2007. Geological studies of igneous rocks and their
855 relationships along the Kyrenia Range. *In*: Moumani, K., Shawabkeh, K., Al-Malabeh, A. &
856 Abdelghafoor, M. (eds) *6th International Congress of Eastern Mediterranean Geology*. Amman,
857 Jordan, 53.

858 Hurley, P.M., Leo, G.W., White, R.W. & Fairbairn, H.W. 1971. Liberian age province (about 2,700
859 my) and adjacent provinces in Liberia and Sierra Leone. *Geological Society of America Bulletin*,
860 **82**, 3483-3490.

861 Innocenti, F., Piero, M., Mazzuoli, R., Pasquare, G. & Villari, L. 1982. *Anatolia and North-Western*
862 *Iran*. Thorpe, R. S. (ed.). Wiley, New York.

863 Juteau, T. 1975. *Les Ophiolites Des Nappes d'Antalya (Taurides Occidentales, Turquie)*. Mémoire
864 de la Sciences de la Terra, Nancy.

865 Karaoğlan, F., Parlak, O., Klötzli, U., Thöni, M. & Koller, F. 2012. U-Pb and Sm-Nd geochronology

of the ophiolites from the SE Turkey: implications for the Neotethyan evolution. *Geodinamica Acta*, **25**, 146-161.

Karaoğlan, F., Parlak, O., Klötzli, U.R.S., Thöni, M. & Koller, F. 2013*a*. U-Pb and Sm-Nd geochronology of the Kızıldağ (Hatay, Turkey) ophiolite: implications for the timing and duration of suprasubduction zone type oceanic crust formation in the southern Neotethys. *Geological Magazine*, **150**, 283-299.

Karaoğlan, F., Parlak, O., Robertson, A., Thöni, M., Klötzli, U., Koller, F. & Okay, A.İ. 2013*b*. Evidence of Eocene high-temperature/high-pressure metamorphism of ophiolitic rocks and granitoid intrusion related to Neotethyan subduction processes (Doğanşehir area, SE Anatolia). *In*: Robertson, A.H.F., Parlak, O. & Ünlügenç, U.C. (eds) *Geological Development of Anatolia and the Easternmost Mediterranean Region*. Geological Society, London, Special Publications, **372**, 249-272.

Karaoğlan, F., Parlak, O., Hejl, E., Neubauer, F. & Kloetzli, U. 2016. The temporal evolution of the active margin along the Southeast Anatolian Orogenic Belt (SE Turkey): Evidence from U-Pb, Ar-Ar and fission track chronology. *Gondwana Research*, **33**, 190-208.

Kelly, N.M., Hinton, R.W., Harley, S.L. & Appleby, S.K. 2008. New SIMS U-Pb zircon ages from the Langavat Belt, South Harris, NW Scotland: Implications for the Lewisian terrane model. *Journal of the Geological Society*, **165**, 967-981.

Kolodner, K., Avigad, D., McWilliams, M., Wooden, J.L., Weissbrod, T. & Feinstein, S. 2006. Provenance of north Gondwana Cambrian-Ordovician sandstone: U-Pb SHRIMP dating of detrital zircons from Israel and Jordan. *Geological Magazine*, **143**, 367-391.

Kröner, A. & Şengör, A.M.C. 1990. Archean and Proterozoic ancestry in late Precambrian to early Paleozoic crustal elements of southern Turkey as revealed by single-zircon dating. *Geology*, **18**, 1186-1190.

Kröner, A., Willner, A.P., Hegner, E., Jaeckel, P. & Nemchin, A. 2001. Single zircon ages, PT evolution and Nd isotopic systematics of high-grade gneisses in southern Malawi and their bearing on the evolution of the Mozambique belt in southeastern Africa. *Precambrian Research*, **109**, 257-291.

Lapierre, H. 1975. *Les Formations Sédimentaires et Éruptives Des Nappes de Mamonia et Leurs Relations Avec Le Massif Du Troodos (Chypre Occidentale)*. Mémoires de la Société

géologique de France.

Liégeois, J.-P., Black, R., Navez, J. & Latouche, L. 1994. Early and late Pan-African orogenies in the Air assembly of terranes (Tuareg Shield, Niger). *Precambrian Research*, **67**, 59-88.

Linnemann, U., McNaughton, N.J., Romer, R.L., Gehmlich, M., Drost, K. & Tonk, C. 2004. West African provenance for Saxo-Thuringia (Bohemian Massif): Did Armorica ever leave pre-Pangean Gondwana? - U/Pb-SHRIMP zircon evidence and the Nd-isotopic record. *International Journal of Earth Sciences*, **93**, 683-705.

Livermore, R.A. & Smith, A.G. 1985. Some boundary conditions for the evolution of the Mediterranean region. *In*: Stanley, D. J. & Wezel, F.-C. (eds) *Geological Evolution of the Mediterranean Basin*. Springer, 83-98.

Lord, A.R., Panayides, I., Urquhart, E. & Xenophontos, C. 2000. A biochronostratigraphical framework for the Late Cretaceous-Recent circum-Troodos sedimentary sequence, Cyprus. *In*: Panayides, I., Xenophontos, C. & Malpas, J. (eds) *Proceedings of the Third International Conference on the Geology of the Eastern Mediterranean*. Cyprus Geological Survey Department, Nicosia, Cyprus, 289-298.

Ludwig, K.R. 2012. Users manual for Isoplot 3.75. *Berkeley Geochronology Centre Special Publication No. 5*, 1-75.

Mackintosh, P.W. & Robertson, A.H.F. 2012. Late Devonian-Late Triassic sedimentary development of the central Taurides, S Turkey: Implications for the northern margin of Gondwana. *Gondwana Research*, **21**, 1089-1114.

Mackintosh, P.W. & Robertson, A.H.F. 2013. Sedimentary and structural evidence for two-phase Upper Cretaceous and Eocene emplacement of the Tauride thrust sheets in central southern Turkey. *In*: Robertson, A.H.F., Parlak, O. & Ünlügenç, U.C. (eds) *Geological Development of Anatolia and the Easternmost Mediterranean Region*. Geological Society, London, Special Publications, **372**, 299-322.

McCay, G.A. & Robertson, A.H.F. 2012. Late Eocene-Neogene sedimentary geology of the Girne (Kyrenia) Range, northern Cyprus: A case history of sedimentation related to progressive and diachronous continental collision. *Sedimentary Geology*, **265**-**266**, 30-55.

McCay, G.A. & Robertson, A.H.F. 2013. Upper Miocene-Pleistocene deformation of the Girne

925 (Kyrenia) Range and Dar Dere (Ovgos) lineaments, northern Cyprus: role in collision and
926 tectonic escape in the easternmost Mediterranean region. *In*: Robertson, A.H.F., Parlak, O. &
927 Ünlügenç, U.C. (eds) *Geological Development of Anatolia and the Easternmost Mediterranean*
928 *Region*. Geological Society, London, Special Publications, **372**, 421-445.

929 McCay, G.A., Robertson, A.H.F., Kroon, D., Raffi, I., Ellam, R.M. & Necdet, M. 2013. Stratigraphy
930 of Cretaceous to Lower Pliocene sediments in the northern part of Cyprus based on comparative
931 $^{87}Sr/^{86}Sr$ isotopic, nannofossil and planktonic foraminiferal dating. *Geological Magazine*, **150**,
932 333-359.

933 McLennan, S.M., Bock, B., Compston, W., Hemming, S.R. & McDaniel, D.K. 2001. Detrital zircon
934 geochronology of Taconian and Acadian foreland sedimentary rocks in New England. *Journal*
935 *of Sedimentary Research*, **71**, 305-317.

936 Meert, J.G. & Torsvik, T.H. 2003. The making and unmaking of a supercontinent: Rodinia revisited.
937 *Tectonophysics*, **375**, 261-288.

938 Moores, E.M. & Vine, F.J. 1971. The Troodos Massif, Cyprus and other ophiolites as oceanic crust:
939 evaluation and implications. *Philosophical Transactions of the Royal Society of London. Series*
940 *A, Mathematical and Physical Sciences*, **268**, 443-466.

941 Mukasa, S.B. & Ludden, J.N. 1987. Uranium-lead isotopic ages of plagiogranites from the Troodos
942 ophiolite, Cyprus, and their tectonic significance. *Geology*, **15**, 825-828.

943 Murphy, J.B., Fernández-Suárez, J. & Jeffries, T.E. 2004*a*. Lithogeochemical and Sm-Nd and U-Pb
944 isotope data from the Silurian-Lower Devonian Arisaig Group clastic rocks, Avalon terrane,
945 Nova Scotia: A record of terrane accretion in the Appalachian-Caledonide orogen. *Geological*
946 *Society of America Bulletin*, **116**, 1183-1201.

947 Murphy, J.B., Pisarevsky, S.A., Nance, R.D. & Keppie, J.D. 2004*b*. Neoproterozoic-Early Paleozoic
948 evolution of peri-Gondwanan terranes: implications for Laurentia-Gondwana connections.
949 *International Journal of Earth Sciences*, **93**, 659-682.

950 Murphy, J.B., FernÁndez-SuÁrez, J., Jeffries, T. & Strachan, R. 2004*c*. U-Pb (LA-ICP-MS) dating
951 of detrital zircons from Cambrian clastic rocks in Avalonia: erosion of a Neoproterozoic arc
952 along the northern Gondwanan margin. *Journal of the Geological Society*, **161**, 243-254.

953 Nance, R.D., Murphy, J.B., *et al.* 2008. Neoproterozoic-early Palaeozoic tectonostratigraphy and

palaeogeography of the peri-Gondwanan terranes: Amazonian v. West African connections. *In*: Ennih, N. & Liégeois, J.-P. (eds) *The Boundaries of the West African Craton*. Geological Society, London, Special Publications, **297**, 345-383.

Nurlu, N., Parlak, O., Robertson, A.H.F. & von Quadt, A. 2016. Implications of Late Cretaceous U-Pb zircon ages of granitic intrusions cutting ophiolitic and volcanogenic rocks for the assembly of the Tauride allochthon in SE Anatolia (Helete area, Kahramanmaraş Region, SE Turkey). *International Journal of Earth Sciences*, **105**, 283-314.

Okay, A.I. 2002. Jadeite-chloritoid-glaucophane-lawsonite blueschists in north- west Turkey: unusually high P/T ratios in continental crust. *Journal of Metamorphic Geology*, **20**, 757-768.

Okay, A.I. & Nikishin, A.M. 2015. Tectonic evolution of the southern margin of Laurasia in the Black Sea region. *International Geology Review*, **57**, 1051-1076.

Okay, A.I. & Tüysüz, O. 1999. Tethyan sutures of northern Turkey. *In*: Durand, B., Jolivet, L., Horváth, F. & Séranne, M. (eds) *The Mediterranean Basins: Tertiary Extension within the Alpine Orogen*. Geological Society, London, Special Publications, **156**, 475-515.

Okay, A.I., Bozkurt, E., Satır, M., Yiğitbaş, E., Crowley, Q.G. & Shang, C.K. 2008*a*. Defining the southern margin of Avalonia in the Pontides: geochronological data from the Late Proterozoic and Ordovician granitoids from NW Turkey. *Tectonophysics*, **461**, 252-264.

Okay, A.I., Satır, M. & Shang, C.K. 2008*b*. Ordovician metagranitoid from the Anatolide- Tauride Block, northwest Turkey: geodynamic implications. *Terra Nova*, **20**, 280-288.

Okay, A.I., Tansel, I. & Tüysüz, O. 2001. Obduction, subduction and collision as reflected in the Upper Cretaceous-Lower Eocene sedimentary record of western Turkey. *Geological Magazine*, **138**, 117-142.

Oyan, V. 2018. Ar-Ar dating and petrogenesis of the Early Miocene Taşkapı-Mecitli (Erciş-Van) granitoid, Eastern Anatolia Collisional Zone, Turkey. *Journal of Asian Earth Sciences*, **158**, 210-226.

Özbey, Z., Ustaömer, T., Robertson, A.H.F. & Ustaömer, P.A. 2013. Tectonic significance of Late Ordovician granitic magmatism and clastic sedimentation on the northern margin of Gondwana (Tavşanlı Zone, NW Turkey). *Journal of the Geological Society*, **170**, 159-173.

Özgül, N. 1984. Stratigraphy and tectonic evolution of the central Taurides. *In*: Tekeli, O. &

983 Göncüoğlu, M.C. (eds) *Proceedings of the International Symposium on the Geology of the*
984 *Taurus Belt*. MTA, Ankara, 77-90.

985 Parlak, O. 2006. Geodynamic significance of granitoid magmatism in the southeast Anatolian orogen:
986 geochemical and geochronogical evidence from Göksun-Afşin (Kahramanmaraş, Turkey)
987 region. *International Journal of Earth Sciences*, **95**, 609-627.

988 Parlak, O. & Delaloye, M. 1999. Precise $^{40}Ar/^{39}Ar$ ages from the metamorphic sole of the Mersin
989 ophiolite (southern Turkey). *Tectonophysics*, **301**, 145-158.

990 Parlak, O. & Robertson, A.H.F. 2004. The ophiolite-related Mersin Melange, southern Turkey: its
991 role in the tectonic-sedimentary setting of Tethys in the Eastern Mediterranean region.
992 *Geological Magazine*, **141**, 257-286.

993 Pearce, J.A. 1975. Basalt geochemistry used to investigate past tectonic environments on Cyprus.
994 *Tectonophysics*, **25**, 41-67.

995 Pearce, J.A., Bender, J.F., et al. 1990. Genesis of collision volcanism in Eastern Anatolia, Turkey.
996 *Journal of Volcanology and Geothermal Research*, **44**, 189-229.

997 Perinçek, D. & Kozlu, H. 1984. Stratigraphical and structural relations of the units in the Afşin-
998 Elbistan-Doğanşehir region (Eastern Taurus). *In*: Tekeli, O. & Göncüoğlu, M. C. (eds) *Geology*
999 *of the Taurus Belt*. MTA, Ankara, Proceedings of International Symposium, 181-198.

1000 Rızaoğlu, T., Parlak, O., Hoeck, V. & İşler, F. 2006. Nature and significance of Late Cretaceous
1001 ophiolitic rocks and their relation to the Baskil granitic intrusions of the Elazığ region, SE
1002 Turkey. *In*: Robertson, A.H.F. & Mountrakis, D. (eds) *Tectonic Development of the Eastern*
1003 *Mediterranean Region*. Geological Society, London, Special Publications, **260**, 327-350.

1004 Rızaoğlu, T., Parlak, O., Höck, V., Koller, F., Hames, W.E. & Billor, Z. 2009. Andean-type active
1005 margin formation in the eastern Taurides: Geochemical and geochronogical evidence from the
1006 Baskil granitoid (Elazığ, SE Turkey). *Tectonophysics*, **473**, 188-207.

1007 Robertson, A.H.F. 1977. The Moni Melange, Cyprus: an olistostrome formed at a destructive plate
1008 margin. *Journal of the Geological Society*, **133**, 447-466.

1009 Robertson, A.H.F. 1998. Tectonic significance of the Eratosthenes Seamount: a continental fragment
1010 in the process of collision with a subduction zone in the eastern Mediterranean (Ocean Drilling
1011 Program Leg 160). *Tectonophysics*, **298**, 63-82.

1012 Robertson, A.H.F. 2002. Overview of the genesis and emplacement of Mesozoic ophiolites in the
1013 Eastern Mediterranean Tethyan region. *Lithos*, **65**, 1-67.

1014 Robertson, A.H.F. & Dixon, J.E. 1984. Introduction: aspects of the geological evolution of the
1015 Eastern Mediterranean. *In*: Dixon, J.E. & Robertson, A.H.F. (eds) *The Geological Evolution of*
1016 *the Eastern Mediterranean*. Geological Society, London, Special Publications, **17**, 1-74.

1017 Robertson, A.H.F. & Kinnaird, T.C. 2016. Structural development of the central Kyrenia Range
1018 (north Cyprus) in its regional setting in the eastern Mediterranean region. *International Journal*
1019 *of Earth Sciences*, **105**, 417-437.

1020 Robertson, A.H.F. & Ustaömer, T. 2009*a*. Formation of the Late Palaeozoic Konya Complex and
1021 comparable units in southern Turkey by subduction-accretion processes: Implications for the
1022 tectonic development of Tethys in the Eastern Mediterranean region. *Tectonophysics*, **473**, 113-
1023 148.

1024 Robertson, A.H.F. & Ustaömer, T. 2009*b*. Upper Palaeozoic subduction/accretion processes in the
1025 closure of Palaeotethys: Evidence from the Chios Melange (E Greece), the Karaburun Melange
1026 (W Turkey) and the Teke Dere Unit (SW Turkey). *Sedimentary Geology*, **220**, 29-59.

1027 Robertson, A.H.F. & Ustaömer, T. 2011. Role of tectonic-sedimentary melange and Permian-
1028 Triassic cover units, central southern Turkey in Tethyan continental margin evolution. *Journal*
1029 *of Asian Earth Sciences*, **40**, 98-120.

1030 Robertson, A.H.F. & Woodcock, N.H. 1979. Mamonia Complex, southwest Cyprus: Evolution and
1031 emplacement of a Mesozoic continental margin. *Geological Society of America Bulletin*, **90**,
1032 651-665.

1033 Robertson, A.H.F. & Woodcock, N.H. 1981*a*. Alakır Çay Group, Antalya complex, SW Turkey: A
1034 deformed Mesozoic carbonate margin. *Sedimentary Geology*, **30**, 95-131.

1035 Robertson, A.H.F. & Woodcock, N.H. 1981*b*. Bilelyeri Group, Antalya Complex: deposition on a
1036 Mesozoic passive continental margin, south- west Turkey. *Sedimentology*, **28**, 381-399.

1037 Robertson, A.H.F. & Woodcock, N.H. 1981*c*. Gödene Zone, Antalya Complex: volcanism and
1038 sedimentation along a Mesozoic continental margin, SW Turkey. *Geologische Rundschau*, **70**,
1039 1177-1214.

1040 Robertson, A.H.F. & Woodcock, N.H. 1984. The SW segment of the Antalya Complex, Turkey as a

Mesozoic-Tertiary Tethyan continental margin. *In*: Dixon, J.E. & Robertson, A.H.F. (eds) *The Geological Evolution of the Eastern Mediterranean*. Geological Society, London, Special Publications, **17**, 251-271.

Robertson, A.H.F. & Woodcock, N.H. 1986. The role of the Kyrenia Range Lineament, Cyprus, in the geological evolution of the eastern Mediterranean area. *Philosophical Transactions of the Royal Society of London. Series A, Mathematical and Physical Sciences*, **317**, 141-177.

Robertson, A.H.F., Ustaömer, T., Parlak, O., Ünlügenç, U.C., Taşlı, K. & İnan, N. 2006. The Berit transect of the Tauride thrust belt, S Turkey: Late Cretaceous-Early Cenozoic accretionary/collisional processes related to closure of the Southern Neotethys. *Journal of Asian Earth Sciences*, **27**, 108-145.

Robertson, A., Parlak, O., Rizaoğlu, T., Ünlügenç, Ü., İnan, N., Tasli, K. & Ustaömer, T. 2007. Tectonic evolution of the South Tethyan ocean: evidence from the Eastern Taurus Mountains (Elaziğ region, SE Turkey). *In*: Ries, A.C., Butler, R.W.H. & Graham, R.H. (eds) *Deformation of the Continental Crust: The Legacy of Mike Coward*. Geological Society, London, Special Publications, **272**, 231-270.

Robertson, A.H.F., Parlak, O. & Ustaömer, T. 2009. Melange genesis and ophiolite emplacement related to subduction of the northern margin of the Tauride-Anatolide continent, central and western Turkey. *In*: Hinsbergen, D. J. J., Edwards, M. A. & Govers, R. (eds) *Collision and Collapse at the Africa-Arabia-Eurasia Subduction Zone*. Geological Society, London, Special Publication, **311**, 9-66.

Robertson, A.H.F., Parlak, O. & Ustaömer, T. 2012*a*. Overview of the Palaeozoic-Neogene evolution of Neotethys in the Eastern Mediterranean region (southern Turkey, Cyprus, Syria). *Petroleum Geoscience*, **18**, 381-404.

Robertson, A.H.F., Tasli, K. & İnan, N. 2012*b*. Evidence from the Kyrenia Range, Cyprus, of the northerly active margin of the Southern Neotethys during Late Cretaceous-Early Cenozoic time. *Geological Magazine*, **149**, 264-290.

Robertson, A.H.F., McCay, G.A., Tasli, K. & Yıldız, A. 2014. Eocene development of the northerly active continental margin of the Southern Neotethys in the Kyrenia Range, north Cyprus. *Geological Magazine*, **151**, 692-731.

Robertson, A.H.F., Parlak, O., Yıldırım, N., Dumitrica, P. & Taslı, K. 2016. Late Triassic rifting and

Jurassic-Cretaceous passive margin development of the Southern Neotethys: evidence from the Adıyaman area, SE Turkey. *International Journal of Earth Sciences*, **105**, 167-201.

Robinson, P.T. & Malpas, J. 1990. The Troodos ophiolite of Cyprus: new perspectives on its origin and emplacement. *In*: Malpas, J., Moores, E. M., Panayiotou, A. & Xenophontos, C. (eds) *Ophiolites, Oceanic Crustal Analogues*. The Geological Survey Department, Nicosia, 13-26.

Rubatto, D. 2002. Zircon trace element geochemistry: partitioning with garnet and the link between U-Pb ages and metamorphism. *Chemical geology*, **184**, 123-138.

Savostin, L.A., Sibuet, J.-C., Zonenshain, L.P., Le Pichon, X. & Roulet, M.-J. 1986. Kinematic evolution of the Tethys belt from the Atlantic Ocean to the Pamirs since the Triassic. *Tectonophysics*, **123**, 1-35.

Seghedi, I. & Helvacı, C. 2016. Early Miocene Kırka-Phrigian Caldera, western Turkey (Eskişehir province), preliminary volcanology, age and geochemistry data. *Journal of Volcanology and Geothermal Research*, **327**, 503-519.

Şengör, A.M.C. 1984. The Cimmeride Orogenic System and the Tectonics of Eurasia. *In*: Şengör, A. M. C. (ed.) *The Cimmeride Orogenic System and the Tectonics of Eurasia*. Geological Society of America, Special Papers, **195**, 1-82.

Şengör, A.M.C. & Yılmaz, Y. 1981. Tethyan evolution of Turkey: a plate tectonic approach. *Tectonophysics*, **75**, 181-241.

Sickmann, Z.T., Schwartz, T.M. & Graham, S.A. 2018. Refining stratigraphy and tectonic history using detrital zircon maximum depositional age: an example from the Cerro Fortaleza Formation, Austral Basin, southern Patagonia. *Basin Research*, **30**, 708-729.

Sircombe, K.N. 2004. AgeDisplay: an EXCEL workbook to evaluate and display univariate geochronological data using binned frequency histograms and probability density distributions. *Computers & Geosciences*, **30**, 21-31.

Stacey, J.S. & Hedge, C.E. 1984. Geochronologic and isotopic evidence for early Proterozoic crust in the eastern Arabian Shield. *Geology*, **12**, 310-313.

Stampfli, G.M. & Borel, G.D. 2002. A plate tectonic model for the Paleozoic and Mesozoic constrained by dynamic plate boundaries and restored synthetic oceanic isochrons. *Earth and Planetary Science Letters*, **196**, 17-33.

1100 Stern, R.J. 1994. Arc assembly and continental collision in the Neoproterozoic East African Orogen:
1101 implications for the consolidation of Gondwanaland. *Annual Review of Earth and Planetary*
1102 *Sciences*, **22**, 319-351.

1103 Sunal, G., Satir, M., Natal'in, B.A. & Toraman, E. 2008. Paleotectonic Position of the Strandja
1104 Massif and Surrounding Continental Blocks Based on Zircon Pb-Pb Age Studies. *International*
1105 *Geology Review*, **50**, 519-545.

1106 Swarbrick, R.E. & Robertson, A.H.F. 1980. Revised stratigraphy of the Mesozoic rocks of southern
1107 Cyprus. *Geological Magazine*, **117**, 547-563.

1108 Tassinari, C.C.G. & Macambira, M.J.B. 1999. Geochronological provinces of the Amazonian Craton.
1109 *Episodes-Newsmagazine of the International Union of Geological Sciences*, **22**, 174-182.

1110 Teipel, U., Eichhorn, R., Loth, G., Rohrmüller, J., Höll, R. & Kennedy, A. 2004. U-Pb SHRIMP and
1111 Nd isotopic data from the western Bohemian Massif (Bayerischer Wald, Germany):
1112 implications for upper Vendian and lower Ordovician magmatism. *International Journal of*
1113 *Earth Sciences*, **93**, 782-801.

1114 Topuz, G., Altherr, R., et al. 2010. Carboniferous high-potassium I-type granitoid magmatism in the
1115 Eastern Pontides: The Gümüşhane pluton (NE Turkey). *Lithos*, **116**, 92-110.

1116 Torley, J.M. & Robertson, A.H.F. 2018. New evidence and interpretation of facies, provenance and
1117 geochemistry of late Triassic-early Cretaceous Tethyan deep-water passive margin-related
1118 sedimentary rocks (Ayios Photios Group), SW Cyprus in the context of eastern Mediterranean
1119 geodynamics. *Sedimentary Geology*, **377**, 82-110.

1120 Urquhart, E. & Banner, F.T. 1994. Biostratigraphy of the supra-ophiolite sediments of the Troodos
1121 Massif, Cyprus: the Cretaceous Perapedhi, Kannaviou, Moni and Kathikas formations.
1122 *Geological Magazine*, **131**, 499-518.

1123 Ustaömer, P.A., Mundil, R. & Renne, P.R. 2005. U/Pb and Pb/Pb zircon ages for arc-related
1124 intrusions of the Bolu Massif (W Pontides, NW Turkey): evidence for Late Precambrian
1125 (Cadomian) age. *Terra Nova*, **17**, 215-223.

1126 Ustaömer, P.A., Ustaömer, T., Collins, A.S. & Robertson, A.H.F. 2009. Cadomian (Ediacaran-
1127 Cambrian) arc magmatism in the Bitlis Massif, SE Turkey: Magmatism along the developing
1128 northern margin of Gondwana. *Tectonophysics*, **473**, 99-112.

1129 Usta ömer, P.A., Usta ömer, T., Gerdes, A. & Zulauf, G. 2011. Detrital zircon ages from a Lower
1130 Ordovician quartzite of the Istanbul exotic terrane (NW Turkey): evidence for Amazonian
1131 affinity. *International Journal of Earth Sciences*, **100**, 23-41.

1132 Usta ömer, P.A., Usta ömer, T., Gerdes, A., Robertson, A.H.F. & Collins, A.S. 2012*a*. Evidence of
1133 Precambrian sedimentation/magmatism and Cambrian metamorphism in the Bitlis Massif, SE
1134 Turkey utilising whole-rock geochemistry and U-Pb LA-ICP-MS zircon dating. *Gondwana*
1135 *Research*, **21**, 1001-1018.

1136 Usta ömer, P.A., Usta ömer, T. & Robertson, A.H.F. 2012*b*. Ion probe U-Pb dating of the Central
1137 Sakarya basement: a peri-Gondwana terrane intruded by late Lower Carboniferous
1138 subduction/collision-related granitic rocks. *Turkish Journal of Earth Sciences*, **21**, 905-932.

1139 Usta ömer, P.A., Usta ömer, T., Gerdes, A., Robertson, A.H.F. & Zulauf, G. 2014. Discovery of a
1140 Triassic magmatic arc source for the Permo-Triassic Karakaya subduction complex, NW
1141 Turkey. *EGU General Assembly Conference Abstracts*, **16**, 9548.

1142 Usta ömer, T., Gerdes, A., Usta ömer, P.A. & Robertson, A. 2012. U-Pb LA-SF-ICP-MS dating of
1143 detrital zircons from an Upper Carboniferous quartzite in the Siyah Aladağ Nappe, Yahyalı-
1144 Kayseri, E Taurides: Source area characteristics. *Paleozoic of Northern Gondwana and Its*
1145 *Petroleum Potential A Field Workshop*, Kayseri, Turkey, 108-110.

1146 Usta ömer, T., Robertson, A.H.F., Usta ömer, P.A., Gerdes, A. & Peytcheva, I. 2013. Constraints on
1147 Variscan and Cimmerian magmatism and metamorphism in the Pontides (Yusufeli-Artvin area),
1148 NE Turkey from U-Pb dating and granite geochemistry. *In*: Robertson, A.H.F., Parlak, O. &
1149 Ünl ügen ç, U.C. (eds) *Geological Development of Anatolia and the Easternmost Mediterranean*
1150 *Region*. Geological Society, London, Special Publications, **372**, 49-74.

1151 Usta ömer, T., Usta ömer, P.A., Robertson, A.H.F., Gerdes, A. & Zulauf, G. 2014. Triassic arc-
1152 derived detritus in the Triassic Karakaya accretionary complex was not derived from either the
1153 S Eurasian margin (Istanbul terrane) or the N Gondwana margin (Taurides). *EGU General*
1154 *Assembly Conference Abstracts*, **16**, 10091.

1155 Usta ömer, T., Usta ömer, P.A., Robertson, A. & Gerdes, A. 2016*a*. Testing alternative tectonic
1156 models of Palaeotethys in the E Mediterranean region: new U-Pb and Lu-Hf isotopic analyses
1157 of detrital zircons from Late Carboniferous and Late Triassic sandstones associated with the
1158 Anatolide and Tauride blocks (S Turkey). *EGU General Assembly Conference Abstracts*, **18**,

15469.

Usta ömer, T., Usta ömer, P.A., Robertson, A.H.F. & Gerdes, A. 2016*b*. Implications of U-Pb and Lu-Hf isotopic analysis of detrital zircons for the depositional age, provenance and tectonic setting of the Permian-Triassic Palaeotethyan Karakaya Complex, NW Turkey. *International Journal of Earth Sciences*, **105**, 7-38.

Usta ömer, T., Usta ömer, P.A., Robertson, A. & Gerdes, A. 2018. U-Pb and Lu-Hf isotopic data from detrital zircons in Late Carboniferous and Late Triassic sandstones used to determine provenance and test alternative tectonic models of the tectonic setting of the Anatolide and Taurides, S Turkey. *GeoBonn 2018*, Bonn, Germany, 65.

Weiler, Y. 1970. Mode of occurrence of pelites in the Kythrea flysch basin (Cyprus). *Journal of Sedimentary Research*, **40**, 1255-1261.

Wiedenbeck, M., Alle, P., et al. 1995. Three natural zircon standards for U- Th- Pb, Lu- Hf, trace element and REE analyses. *Geostandards Newsletter*, **19**, 1-23.

Winchester, J., Pharaoh, T., Verniers, J., Ioane, D. & Seghedi, A. 2006. Palaeozoic accretion of Gondwana-derived terranes to the East European Craton: recognition of detached terrane fragments dispersed after collision with promontories. *In*: Gee, D.G. & Stephenson, R.A. (eds) *European Lithosphere Dynamics*. Geological Society, London, Memoirs, **32**, 323-332.

Yağmurlu, F., Savaşğin, Y. & Ergün, M. 1997. Relation of alkaline volcanism and active tectonism within the evolution of the Isparta Angle, SW Turkey. *The Journal of Geology*, **105**, 717-728.

Yiğitbaş, E., Kerrich, R., Yılmaz, Y., Elmas, A. & Xie, Q. 2004. Characteristics and geochemistry of Precambrian ophiolites and related volcanics from the İstanbul-Zonguldak Unit, Northwestern Anatolia, Turkey: Following the missing chain of the Precambrian South European suture zone to the east. *Precambrian Research*, **132**, 179-206.

Yılmaz, Y. 1993. New evidence and model on the evolution of the southeast Anatolian orogen. *Geological Society of America Bulletin*, **105**, 251-271.

Yılmaz, Y., Tüysüz, O., Yiğitbaş, E., Can Genç, S. & Şengör, A.M.C. 1997. Geology and tectonic evolution of the Pontides. *In*: Robinson, A. G. (ed.) *Regional and Petroleum Geology of the Black Sea and Surrounding Region*. American Association of Petroleum Geologists Memoir 68, 183-226.

1188 Zitter, T.A.C., Woodside, J.M. & Mascle, J. 2003. The Anaximander Mountains: a clue to the
1189 tectonics of southwest Anatolia. *Geological Journal*, **38**, 375-394.

1190 Zlatkin, O., Avigad, D. & Gerdes, A. 2013. Evolution and provenance of Neoproterozoic basement
1191 and Lower Paleozoic siliciclastic cover of the Menderes Massif (western Taurides): Coupled U-
1192 Pb-Hf zircon isotope geochemistry. *Gondwana Research*, **23**, 682-700.

1193 Zulauf, G., Romano, S., Dorr, W. & Fiala, J. 2007. Crete and the Minoan terranes: Age constraints
1194 from U-Pb dating of detrital zircons. *In*: Linnemann, U., Nance, R.D., Kraft, P. & Zulauf, G.
1195 (eds) *The Evolution of the Rheic Ocean: From Avalonian-Cadomian Active Margin to*
1196 *Alleghenian-Variscan Collision*. Geological Society of America, Special Papers, **423**, 401-411.

1197

1198

Figure captions

Fig. 1. Simplified geological map of Cyprus, indicating the locations of the Mamonia Complex (W Cyprus), the Moni Melange (S Cyprus) and the Kyrenia Range (N Cyprus) (modified from McCay & Robertson 2012).

Fig. 2. Outline tectonic map of the Eastern Mediterranean region including North Africa and much of Turkey indicating the main tectonic units mentioned in the text. Main sources: Precambrian basement (Bozkurt *et al.* 1993; Guiraud *et al.* 2001; Yiğitbaş *et al.* 2004; Ustaömer P. A. *et al.* 2005); Paleozoic cover (Göncüoğlu & Kozlu 2000). Note the location of the Mamonia Complex, the Moni Melange and the Kyrenia Range in Cyprus.

Fig. 3. Summary log of the sedimentary Ayios Photios Group, one of the two main tectonic units making up the Mamonia Complex, Cyprus. Note the parts of the succession sampled for zircon dating. Simplified after Torley and Robertson (2018).

Fig. 4. Outline geological map of the Mamonia Complex, showing sample locations in the Ayios Photios Group. Modified after Robertson & Woodcock (1979).

Fig. 5. Outline geological map of part of the Moni Melange showing sample location. Modified after Robertson (1977).

Fig. 6. Summary log of the lithologies making up the Kyrenia Range, Cyprus. Note the parts of the succession sampled for zircon dating. Simplified from Robertson & Woodcock (1986) and McCay & Robertson (2012). Abbreviations: S, south of the Kyrenia Range; N, north of the Kyrenia Range.

Fig. 7. Outline geological map of the Kyrenia Range showing sample locations. Modified after Baroz (1979), Robertson & Woodcock (1986) and Robertson *et al.* (2012*b*).

Fig. 8. Selected cathodoluminescence images of zircon grains analysed from sandstones of the Mamonia Complex (a-c), the Moni Melange (d) and the Kyrenia Range (e-h). Note the analysis spots and corresponding ages ($\pm 1\sigma$ Ma). Scale bar is 20μm.

Fig. 9. (a, c) Concordia diagrams for detrital zircon ages obtained from Late Triassic sandstones (Vlambouros Formation, Mamonia Complex). Inset: enlarged portion of the Concordia diagram for source rock ages from 200-1500, 200-1200 Ma. (b, d) Probability-density distribution of zircon ages from these sandstones. Grey field on the probability-density diagram indicates discordant ages. $^{206}Pb/^{238}U$ is used for ages <1000 Ma and $^{207}Pb/^{206}Pb$ for >1000 Ma.

Fig. 10. (a, c) Concordia diagrams for detrital zircon ages obtained from the Akamas Member (Mamonia Complex) and the Pareklisia Member (Moni Melange). Inset: enlarged portion of the Concordia diagram for source rock ages from 100-1200, 300-1200 Ma. (b, d) Probability-density distribution of zircon ages obtained from these sandstones. Grey field on the probability-density diagram indicates discordant ages. $^{206}Pb/^{238}U$ is used for ages <1000 Ma and $^{207}Pb/^{206}Pb$ for >1000 Ma.

Fig. 11. (a, c) Concordia diagrams for detrital zircon ages obtained from the Late Cretaceous sandstone (Kiparisso Vouno (Alevkaya Tepe) Member) and Eocene sandstone (Kalograia-Ardana (Bahçeli–Ardahan) Formation). Inset: enlarged portion of the Concordia diagram for source rock ages from 0-1100, 0-1200 Ma. (b, d) Probability-density distribution of zircon ages obtained from the above sandstones. The grey field on the probability-density diagram indicates discordant ages. $^{206}Pb/^{238}U$ is used for ages <1000 Ma and $^{207}Pb/^{206}Pb$ for >1000 Ma.

Fig. 12. (a, c) Concordia diagrams for detrital zircon ages obtained from the Miocene sandstones (Davlos (Kaplıca) Formation and Mia Milia (Dağyolu) Formation). Inset: enlarged portion of the Concordia diagram for source rock ages from 0-150, 0-50 Ma. (b, d) Probability-density distribution of zircon ages obtained from the above sandstones. Grey field on the probability-density diagram indicates discordant ages. $^{206}Pb/^{238}U$ is used for ages <1000 Ma and $^{207}Pb/^{206}Pb$ for >1000 Ma.

Fig. 13. Composite successions of the Troodos Massif (including the Moni Melange), the Mamonia Complex and the Kyrenia Range (including their related sedimentary cover). Published ages for the Troodos ophiolite are from Mukasa & Ludden (1987); biostratigraphically dated ages are mainly from Ealey & Knox (1975), Baroz (1979), Urquhart & Banner (1994), Bragin & Krylov (1996, 1999), Hakyemez *et al.* (2000) and Lord *et al.* (2000). Strontium isotopic ages are from McCay *et al.* (2013). Youngest concordant zircon and the proposed main source ages are illustrated for comparison.

Fig. 14. Distribution of detrital zircon ages and/or igneous events known from the major cratons, epi-cratonic basins and peri-Gondwanan terranes. Data source: Amazonia, Friedl *et al.* (2004), Nance *et al.* (2008); Baltica, Linnemann *et al.* (2004); Siberia (Angara), Sunal *et al.* (2008); W Africa, Linnemann *et al.* (2004), Murphy *et al.* (2004*a, b, c*); Arabian-Nubian Shield, Avigad *et al.* (2003), Drost *et al.* (2011); Saharan Metacraton to Tepla-Barrandian, Drost *et al.* (2011) and reference therein; Istanbul terrane, Usta ömer P. A. *et al.* (2011); Central Sakarya, Usta ömer *et al.* (2012*b*); Pontides, Usta ömer *et al.* (2013); Menderes Massif, Kr öner & Şengör (1990), Zulauf *et al.* (2007) and Zlatkin *et al.* (2013); Taurides, Abbo *et al.* (2015); Jordan, Kolodner *et al.* (2006). The numbers

within the bars refer to the number of concordant zircons in the prominent zircon population. Abbreviations: NP, Neoproterozoic; C, Cambrian; Ord., Ordovician; Sil., Silurian; Dev., Devonian; Carb., Carboniferous; P., Permian; Tria., Triassic; TS, Tuareg Shield; BNS, Nenin-Nigeria Shield.

Fig. 15. Tectonic model showing possible provenance and sediment transport of the Ayios Photios Group (Mamonia Complex) in W Cyprus. (a) The Mamonia Complex formed part of the north-Gondwana continent, which rifted during the Triassic. (b) By the Late Triassic, the Mamonia Complex was fully separated from Gondwana and the Tauride platform by the embryonic Southern Neotethys. (c) Passive margin subsidence allowed the accumulation of deep-water, mixed clastic-carbonate slope facies. Abbreviations: s. l., sea level.

Fig. 16. Tectonic model showing the possible provenance and sediment transport of the Late Cretaceous, Middle Eocene and Late Miocene sandstones in the Kyrenia Range. (a) Arc magmatism in the Kyrenia Range during the Campanian. (b) Deposition of terrigenous turbidites (Kiparisso Vouno (Alevkaya Tepe) Member) along the northern, active continental margin of the Southern Neotethys. (c) Deposition of Middle Eocene gravity-flows (Kalograia-Ardana (Bahçeli–Ardahan) Formation) in a foredeep, driven by thrusting to the north of the Kyrenia Range and/or initial continental collision in SE Turkey. (d) Deposition of Late Miocene sandstone turbidites in a foredeep related to closure of the Southern Neotethys. Abbreviations: s. l., sea level; ES, Eratosthenes Seamount.

Supplementary publication

Table S1 Zircon U-Pb dating results of the sandstones analysed from Cyprus.

Figure S1. Histograms show U-Pb analytical zircon data for analysed sandstones from Cyprus. Two main age populations (Ediacaran-Cryogenian, Tonian-Stenian; highlighted with dotted shading) are identified in the sandstones analysed (see text for discussion). Histograms of each sample analysed in this study are shown in Figs. 9-12. Peak ages for the Paleozoic and younger zircons are given as specific numbers besides the columns. Only grains with 90-110% concordance are included. n=number of grains analysed.

Fig. 1

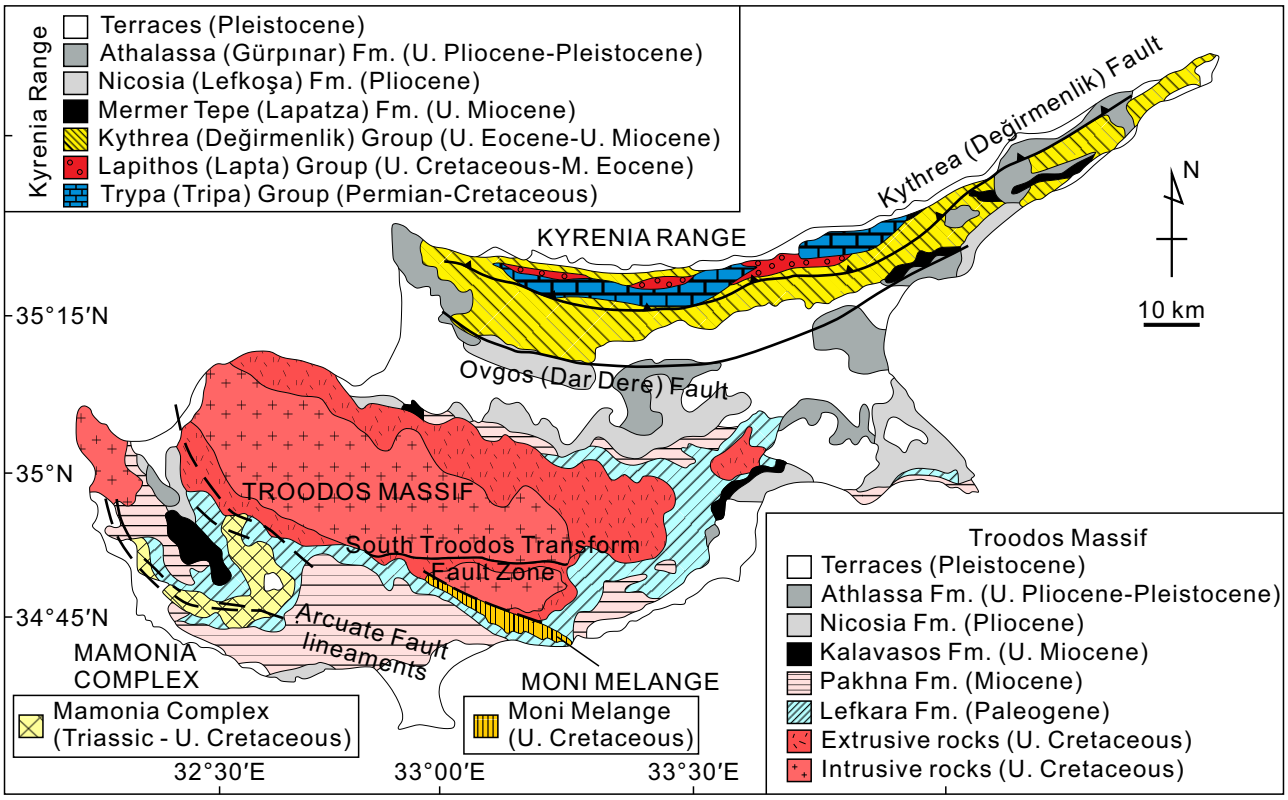

Fig. 2

Click here to access/download;figure;Fig. 2.pdf

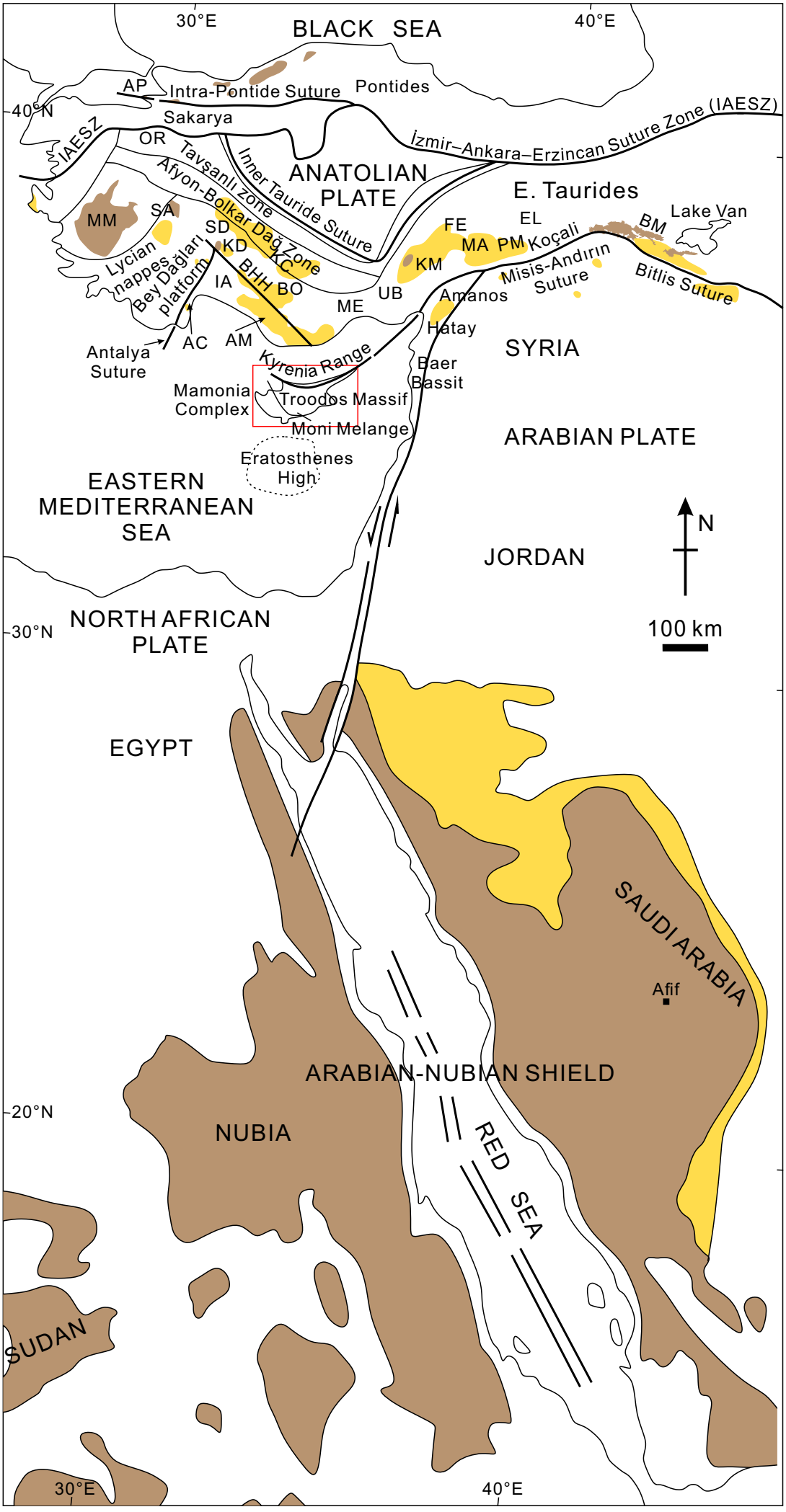

Key

- Late Proterozoic rocks
- Paleozoic rocks
- Suture zone
- Transform fault
- Spreading axis

AC: Antalya Complex
AM: Alanya Massif
AP: Armutlu Peninsula
BO: Bolkar Massif
BHH: Beyşehir-Hoyran-Hadim Nappes
BM: Bitlis Massif
EL: Elazığ
FE: Feke
IA: Isparta Angle
KM: Kahramanmaraş
KC: Konya Complex
KD: Karacahisar dome
MA: Malatya
ME: Mersin ophiolite
MM: Menderes Massif
OR: Orhaneli
PM: Pütürge Massif
SA: Sandıklı
SD: Sultan Dağ
UB: Ulukışla Basin

Fig. 3

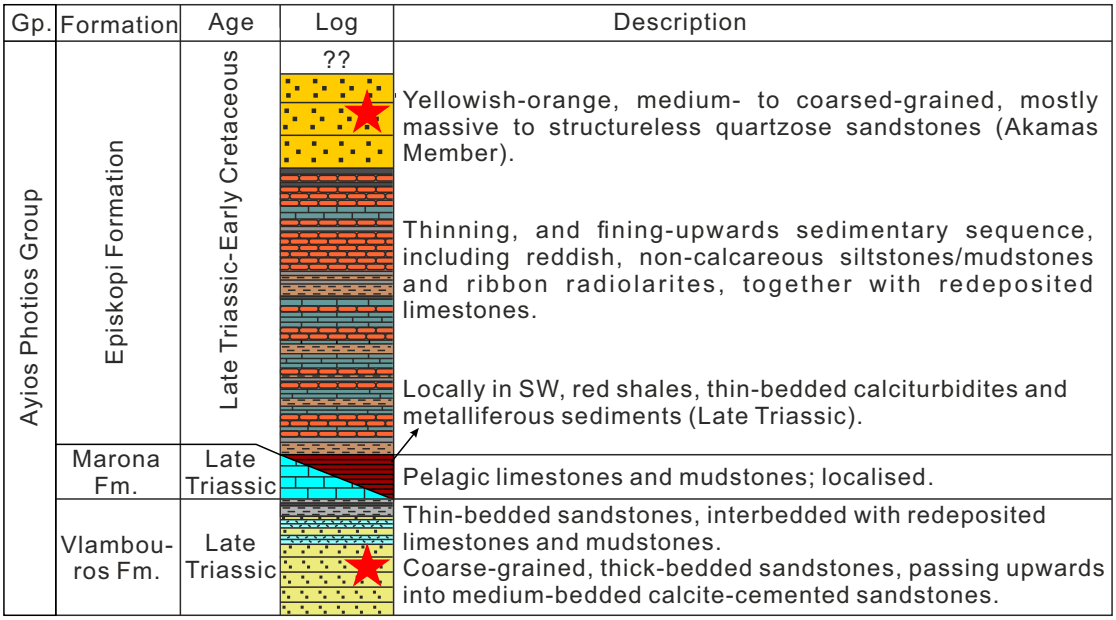

Fig. 4

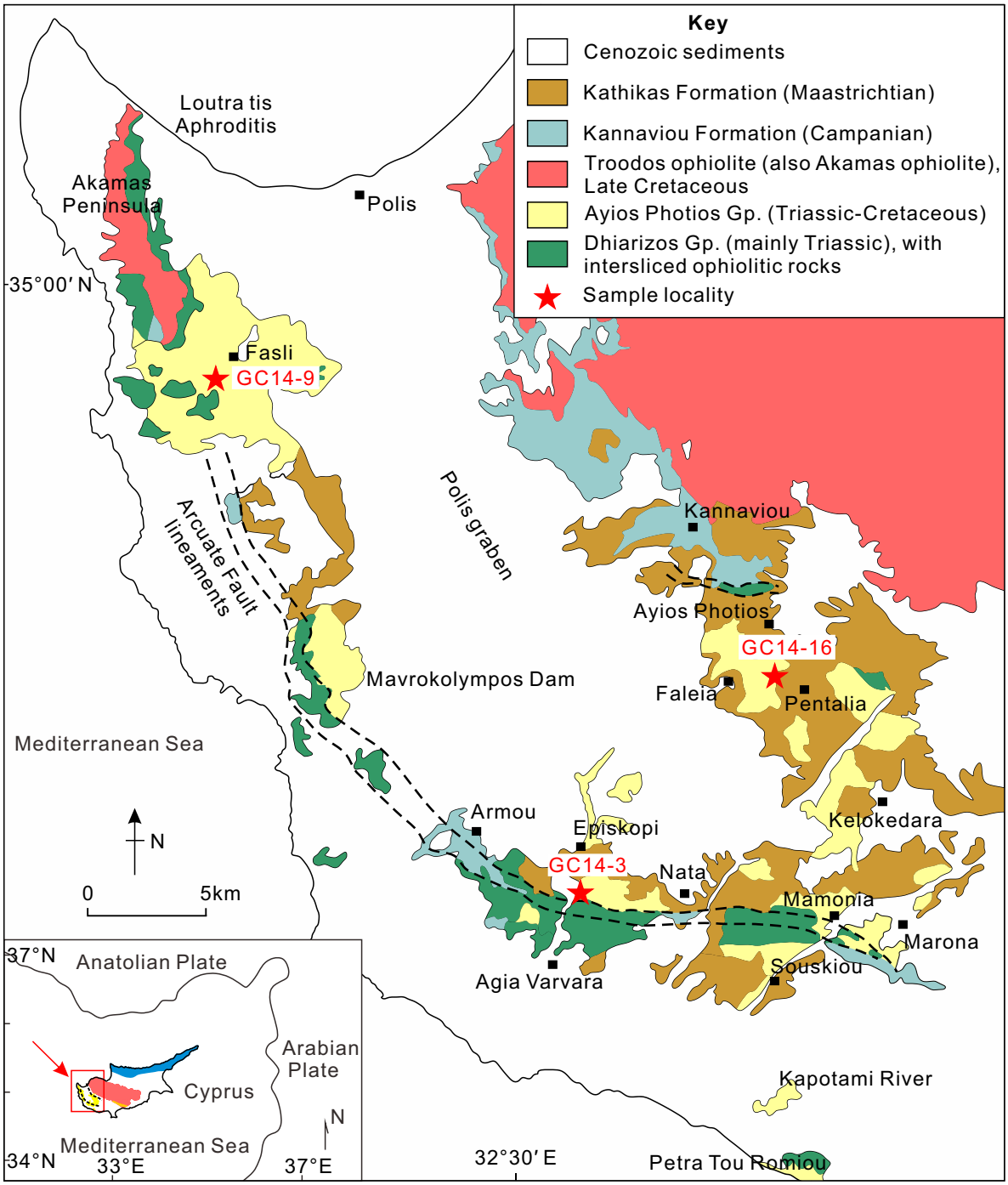

Fig. 5

Click here to access/download;figure;Fig. 5.pdf

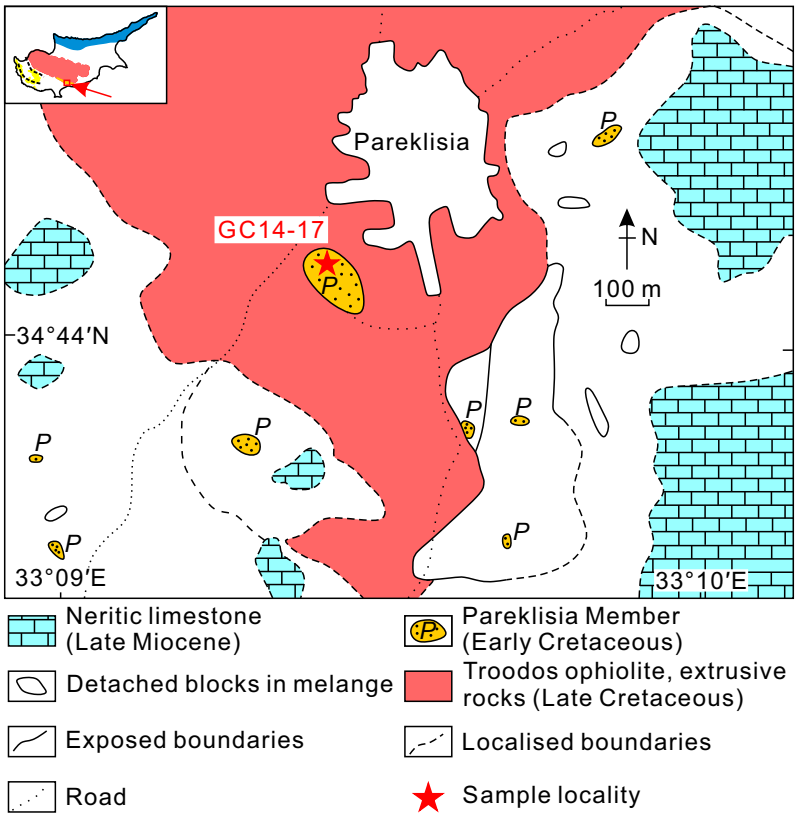

Fig. 6

Click here to access/download;figure;Fig. 6.pdf

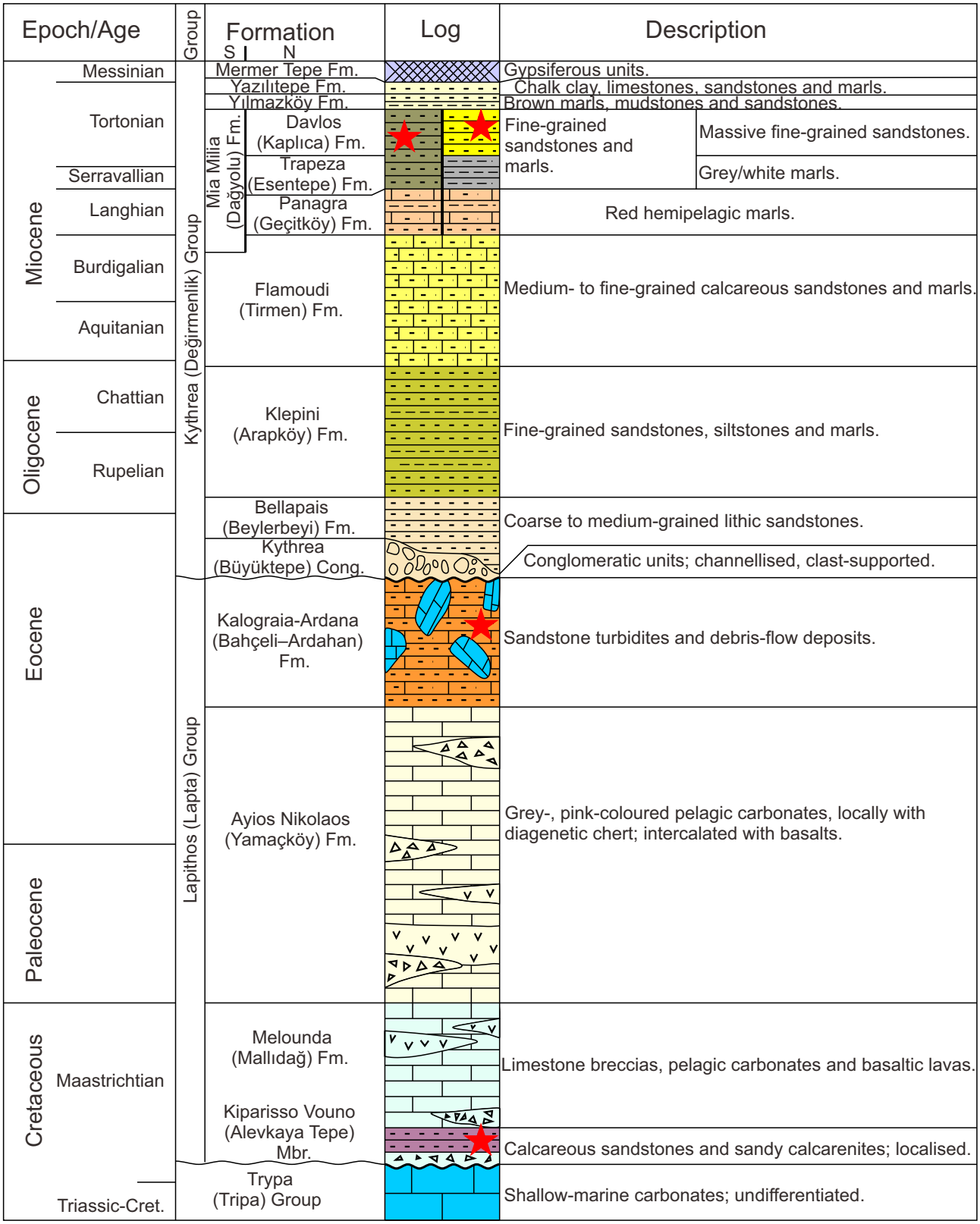

Fig. 7

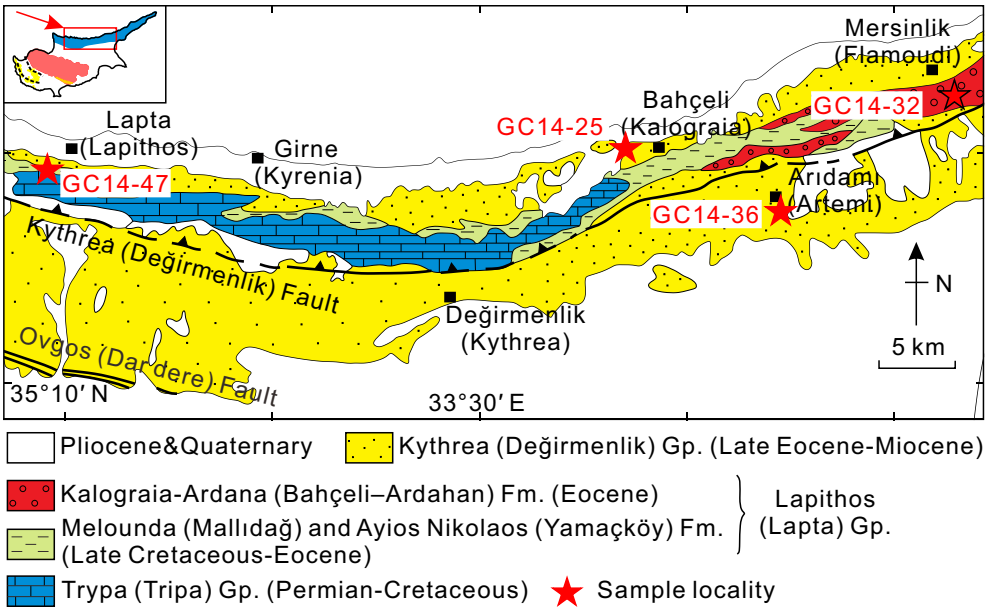

Fig. 8

Click here to access/download;figure;Fig. 8.pdf

Fig. 9

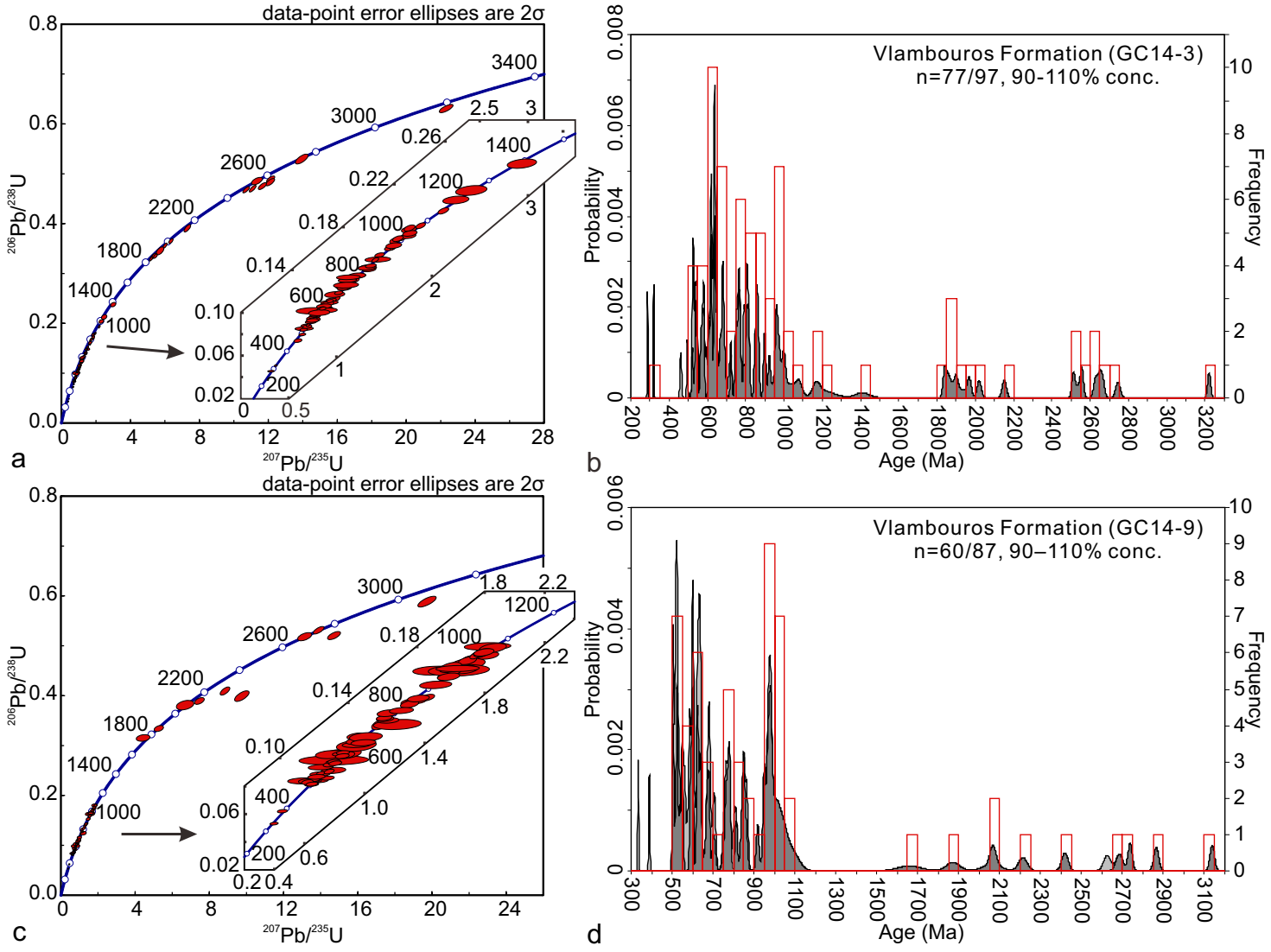

Fig. 10

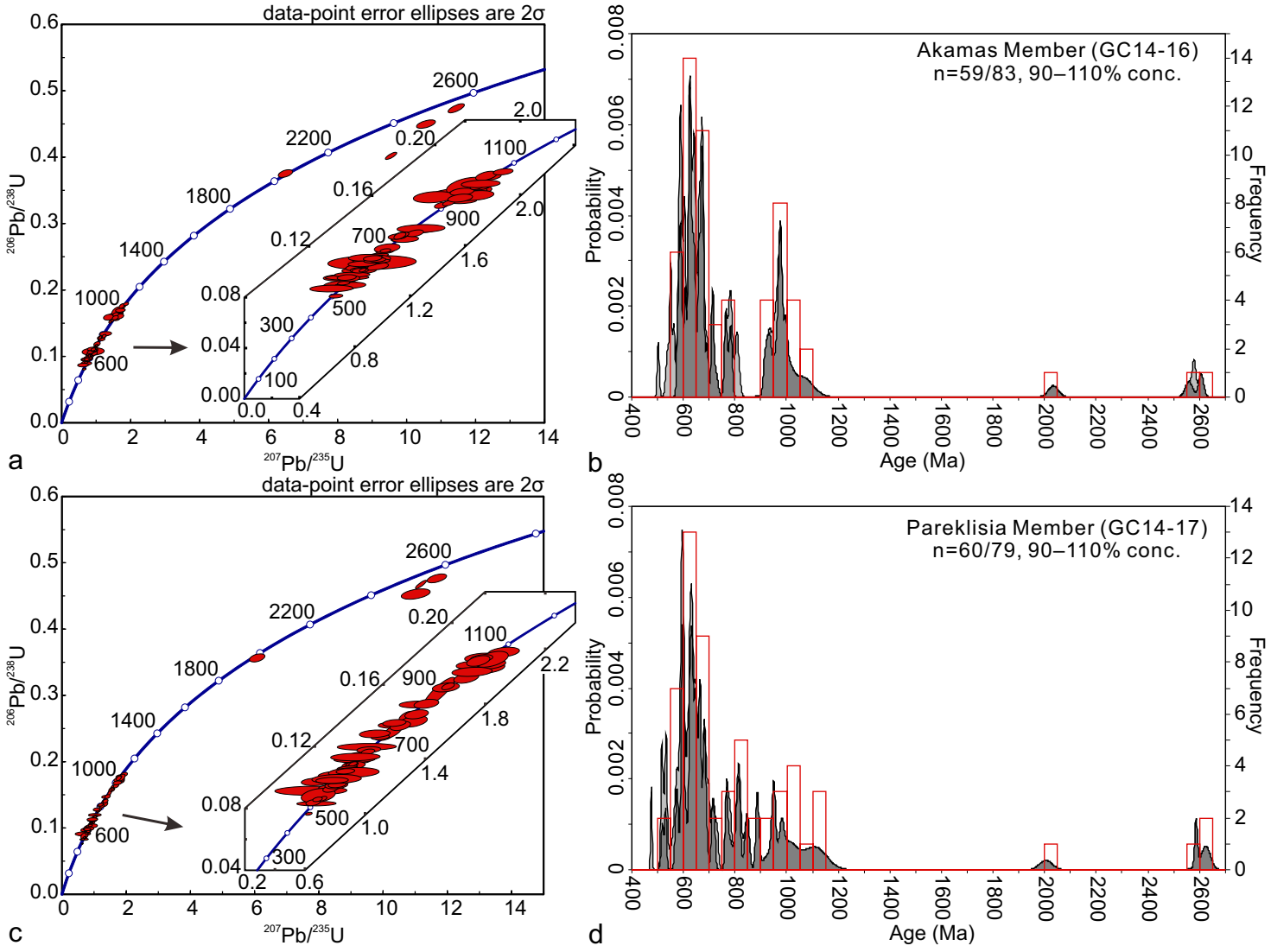

Fig. 11

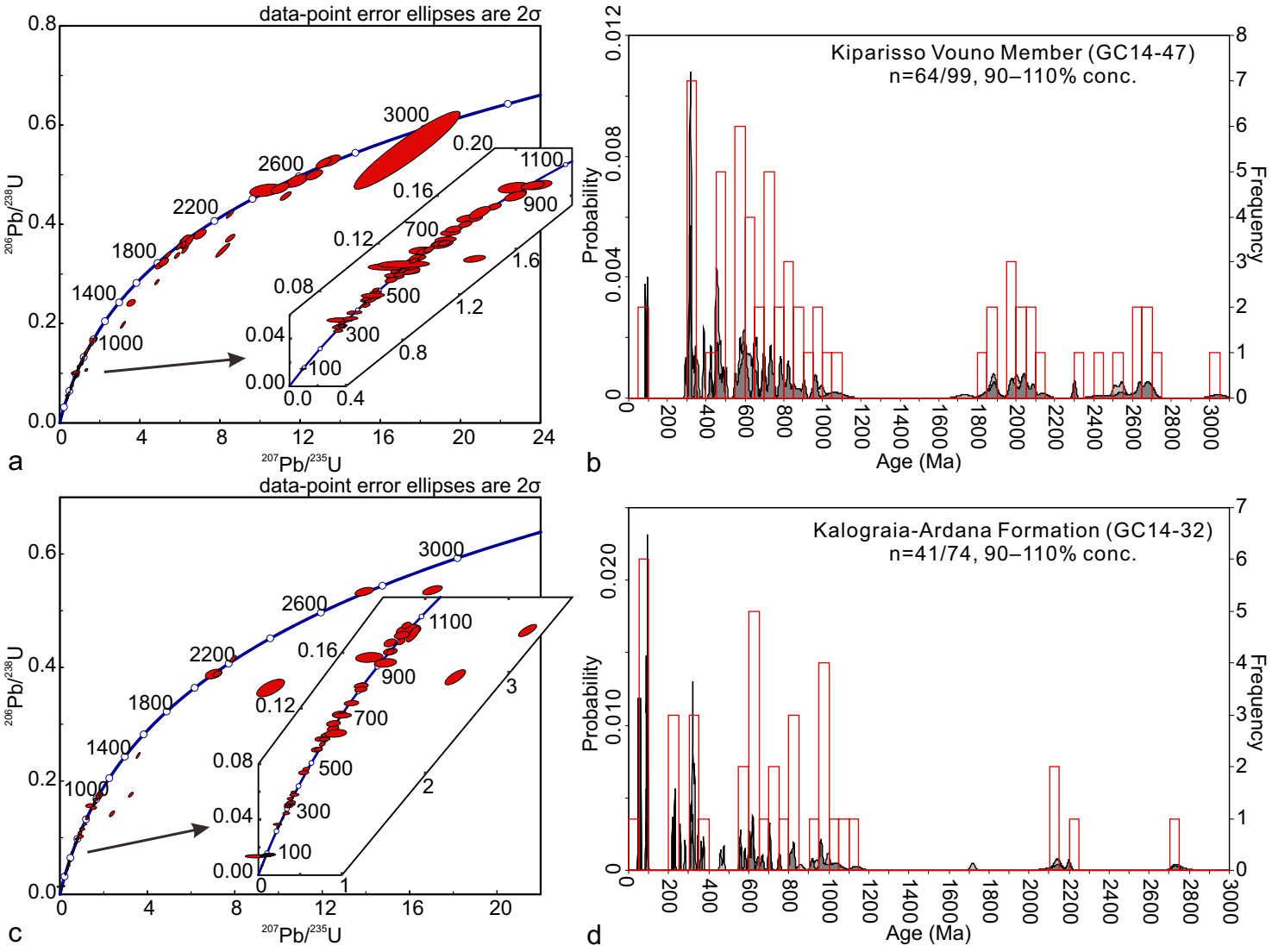

Fig. 12

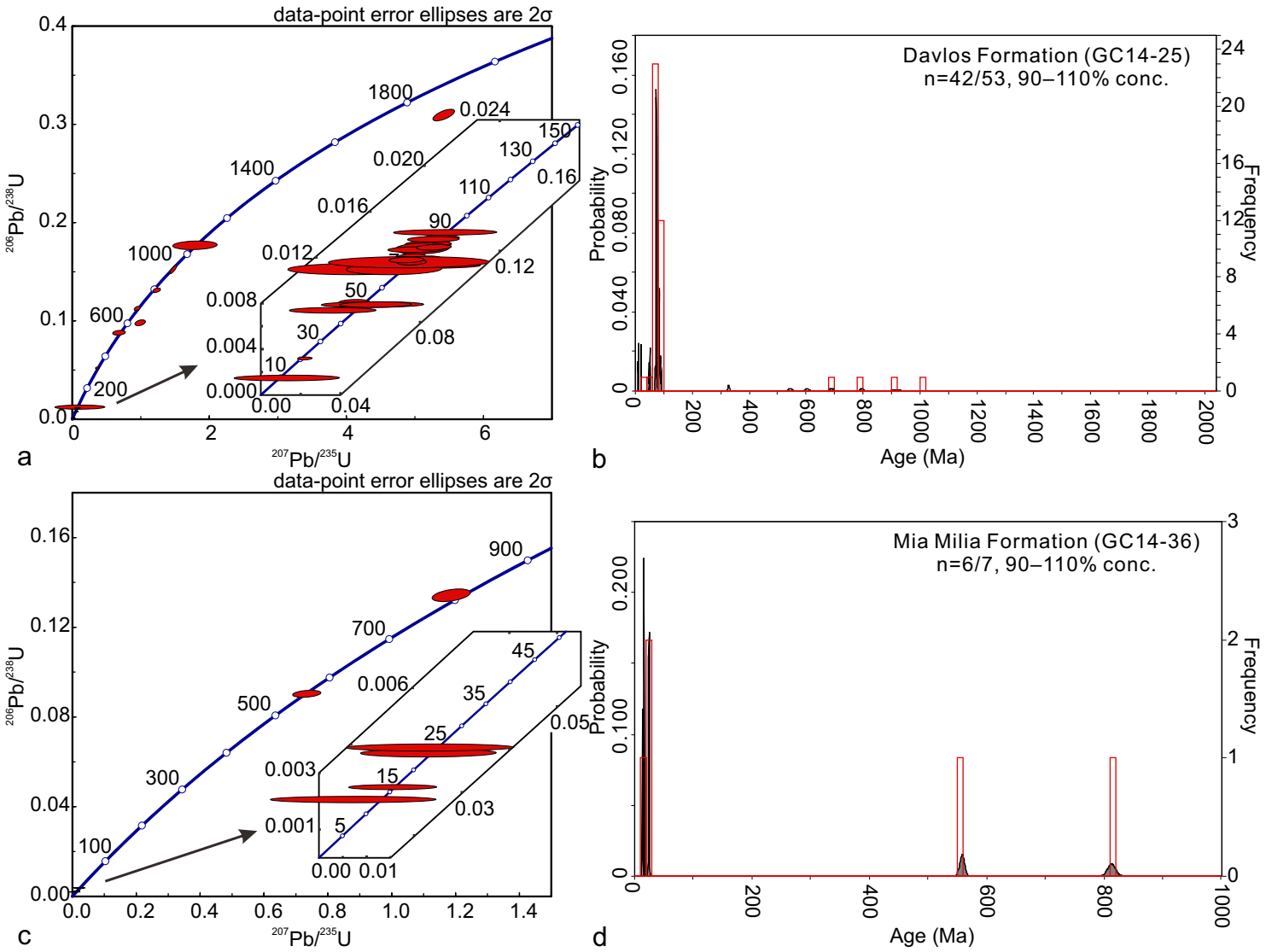

Fig. 13

Click here to access/download;figure;Fig. 13.pdf

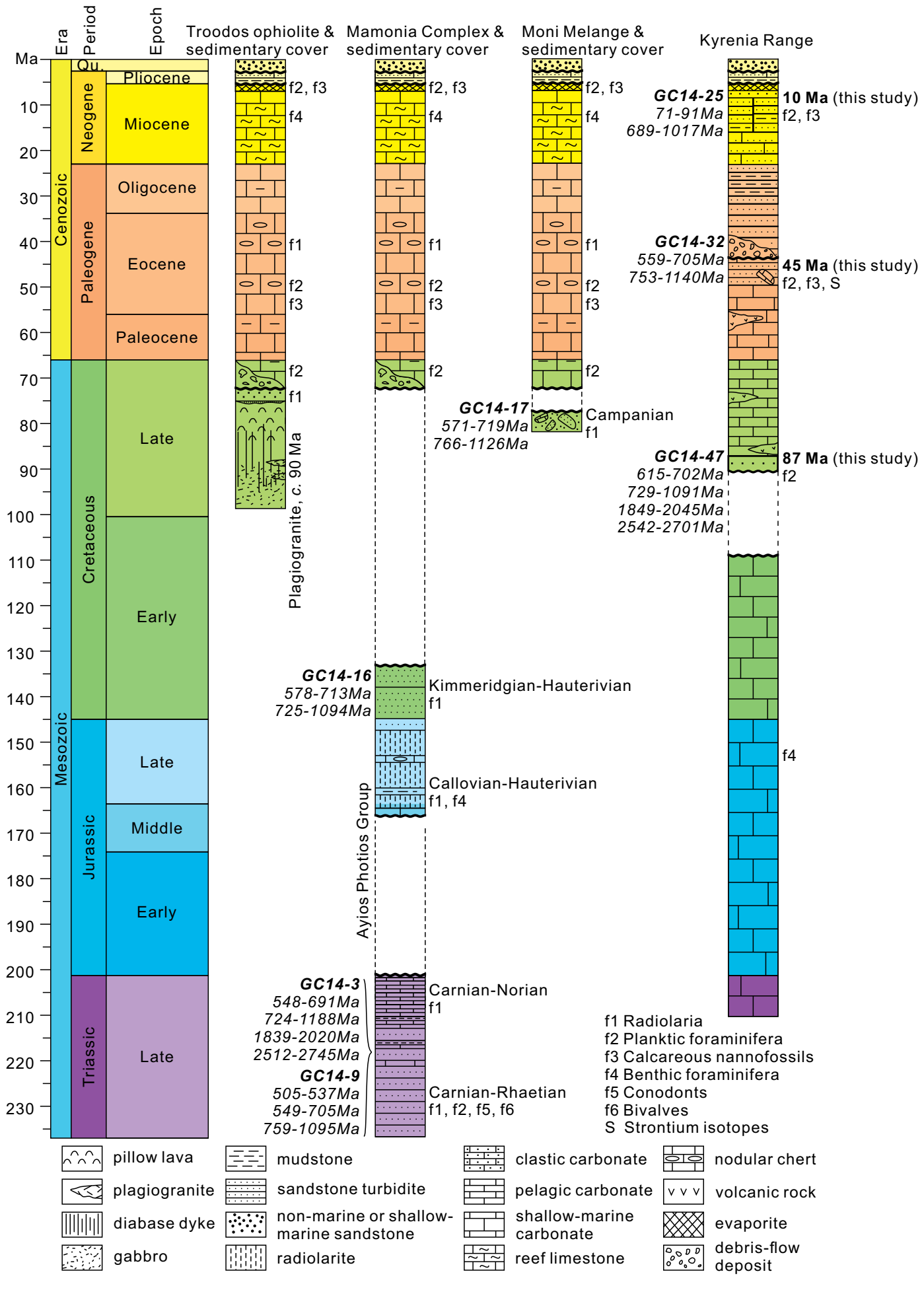

Fig. 14

Click here to access/download;figure;Fig. 14.pdf

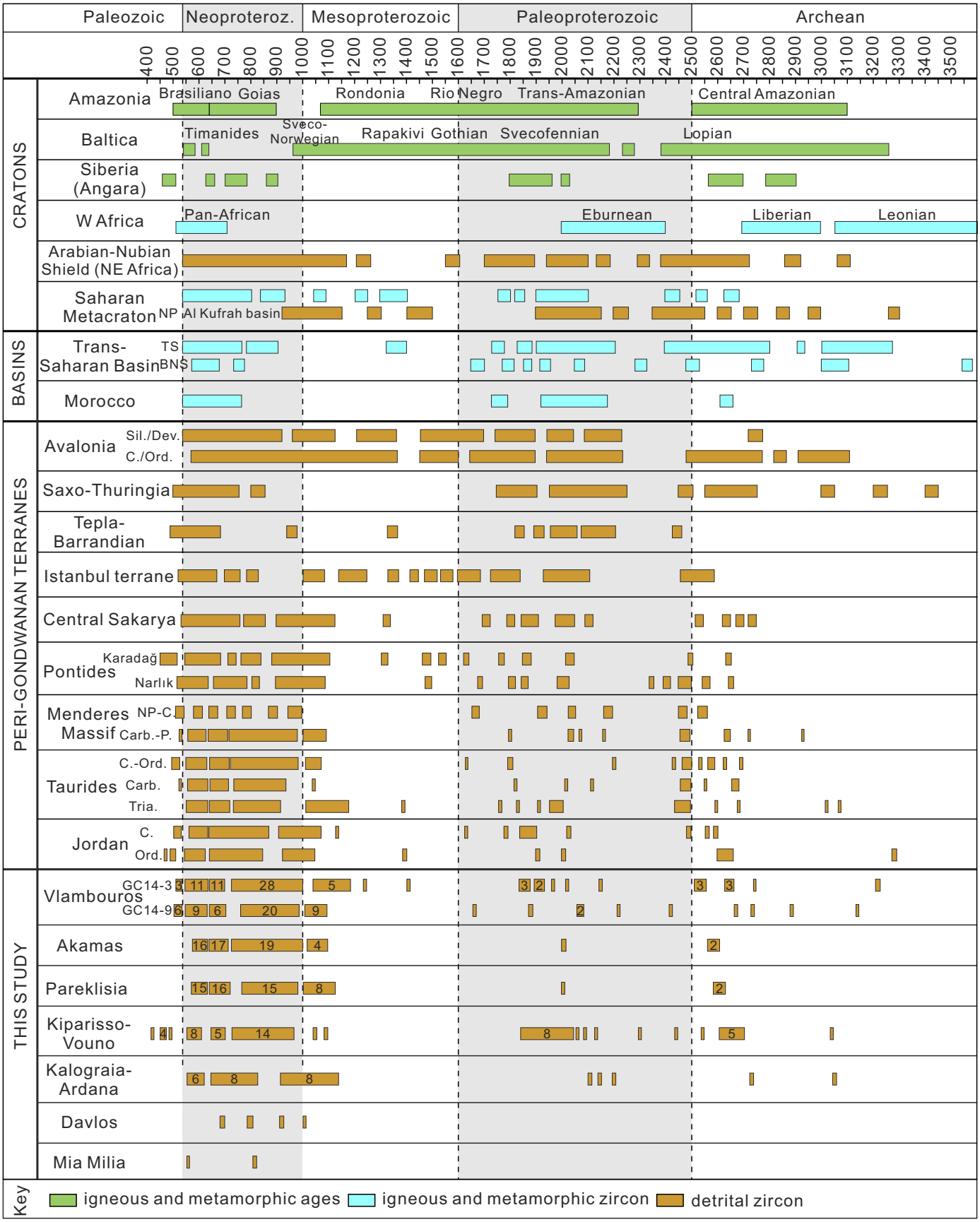

Fig. 15

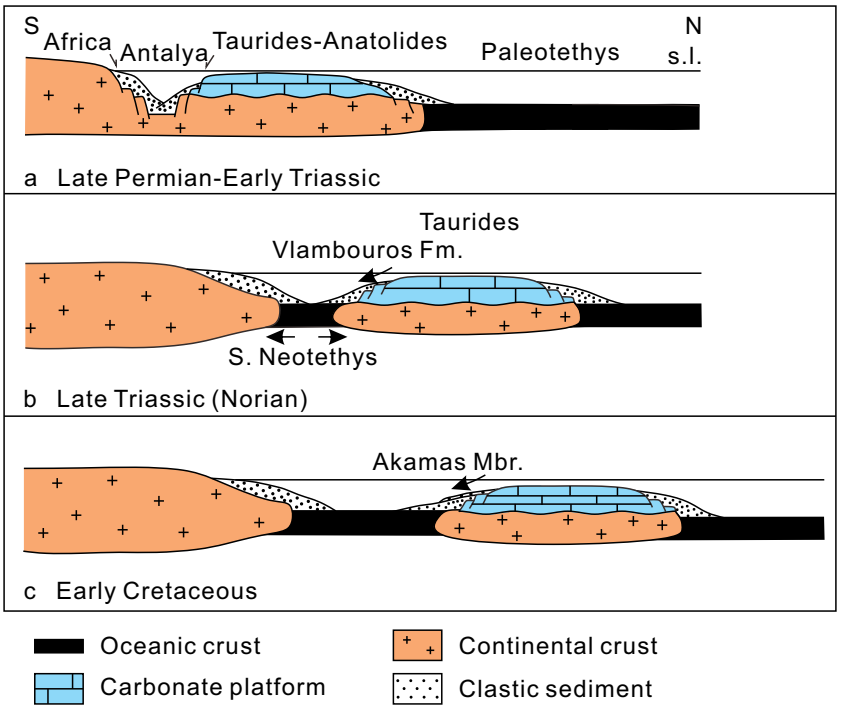

Fig. 16

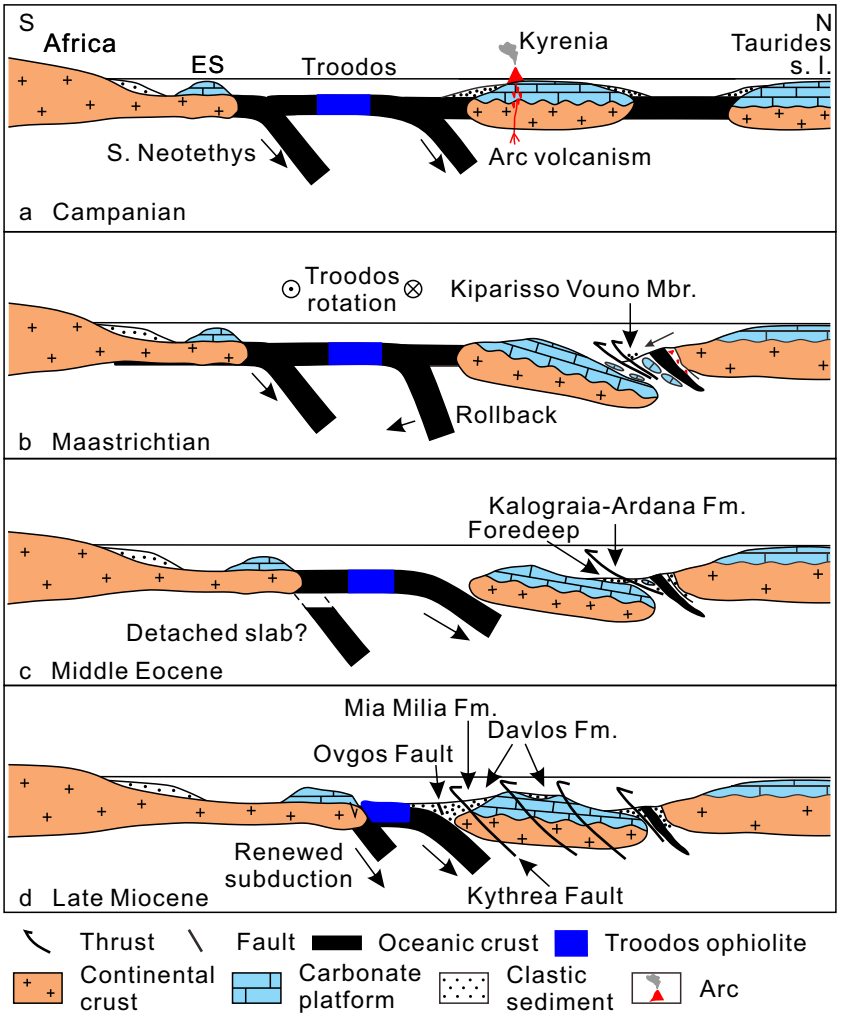

Zircon U-Pb dating results of the sandstones analysed from Cyprus

Histograms show U-Pb analytical zircon data for analysed sandstones from Cyprus